

Reply to review comments

We thank both reviewers for their time and for their constructive comments, which helped to improve the formulation and content of the manuscript.

Listed below are: the reviewers' comments in black, [our reply in blue](#), "[quotes from the originally submitted manuscript in brown](#)" and "[quotes from the revised manuscript in green](#)". All line numbers follow the numbering in the originally submitted manuscript. Figures in the paper are referred to as Fig. 1, Fig. 2, etc. and Figures in this reply as Fig. R1, Fig. R2, etc.

Anonymous Reviewer #1

Received and published: 1 July 2020

The authors compare the contribution of surface temperature and of the ocean circulation changes in response to a moderate radiative perturbation to temperature variations in the deep ocean. This study is welcome as it is often assumed that, in case of a relatively small changes in circulation, the effect of those changes can be neglected and we can consider that the signal at depth can be simply interpreted as the result of the transport of anomalies created at surface by the mean circulation. By doing some well-designed experiments and precise diagnostics, the authors show that this approximation of constant circulation leads to an underestimation of the changes and biases in the timing of warming and cooling at many locations. The manuscript is well-written and provides the adequate information. I have only a few suggestions below on the structure of the paper or to improve the clarity of some parts but none is mandatory for me before publication.

[We thank the reviewer for acknowledging the impact of our manuscript and for the detailed feedback, which improved the clarity and correctness of the text.](#)

General comment

1. I think Table 2 is hard to follow without reading the sup. mat. Furthermore, the uncertainties are very large (as shown by the residuals) and it does not bring much new information. The diagnostic related to water age could be instructive but, except in one case, the value is very small and very uncertain (see lines 306-307 and line 536). I thus suggest to move it to sup. mat. So, all the information related to those diagnostics is grouped at one location. The results could be mentioned in section 3.4 but without details. It also implies that the values of effect one can be computed as given line 528 and display a lower uncertainty.

[Table 2 and most accompanying text is moved to the supplement in a new subsection B5 \(Table 2 is merged here with Table B3\). This shortens Section 3.4. We did not change the values of effect 1 in the table, because that would make it inconsistent, i.e., rows not adding up to 100%. We think the large uncertainty is discussed clearly enough.](#)

Specific comments

1. Line 25. I guess the sentence refers to the ocean depth at the core location but the majority of the cores record changes in SST or near surface temperature changes.

[We changed L24-26 to:](#)

[“\(…\), but oceanic reconstructions below the sea surface are scarce for the last millennium \(Moffa-Sánchez et al., 2019\).”](#)

2. Line 107. I am not sure I understand what is meant by ‘at every surface grid cell are set to a latitude-longitude field’. Does it mean that a constant spatial field is used and the value is different

for each grid cell? Please rephrase.

For every time step we use a new spatial field. We clarified the formulation to:

“[the SST, SSS and sea ice] of surface grid cells are set to the corresponding value in the (latitude, longitude, time step) boundary conditions that are obtained from (...)”

3. Line 115. Maybe I missed something in the procedure but is it possible that a drift occurs just because of the shift to fixed ocean velocities in OcFIX. Is this taken into account?

Switching to FIX mode cannot be the cause of the drift, since we also observed a drift in TRA simulations (before doing the extended spin-up). During fixed-circulation runs, the circulation of every time step of the first simulation year is saved and repeated automatically in subsequent years. Thus the first simulation year should be without forcing, which is ensured by our zero forcing from 1200 to 1223 CE. Small differences in AMOC between simulation year 1 and all subsequent years can occur around the 4th digit, but these are not visible by eye in, e.g., Fig. 2.

4. Line 134. The comparison of results of this study with the ones of Collins et al. is made for different conditions and time periods. Would it be possible to compare the results presented here for the 20th century with the trends for the 20th century simulated in other models for a more meaningful comparison ?

“[about 1750-2000 CE:] This 1.5 Sv AMOC slowdown is within the CMIP5 range of fully coupled AOGCMs and the AMOC in that model mean experiences a similar decrease of 2 Sv from 2000 to 2100 CE under low emission forcing (Collins et al., 2019).”

This is a good point. We now omitted the second part of this sentence. We were mainly interested to compare 1750-2000 CE, because the AMOC slows down in this period in our set-up, but CMIP5 models give a broad range here.

5. Line 141. Isn't it Fig 2a ?

Correct, done. Thank you.

6. Line 166. The link with Fig A3 is not straightforward as you did not explain that it corresponds to tracer concentration while the reader could have imagine that it relates directly to ‘persistent cold anomaly’.

We clarified this.

7. Line 171. Maybe it would be useful to discuss the ventilation rate in the Southern Ocean in the model and its realism as it may have an impact on the results.

We added the following here:

“This ventilation rate in the SO (Fig. 8d and 9d) agrees well with radiocarbon-inferred observations (Gebbie and Huybers, 2012) in the average and maximum SO water age, although qualitatively the Bern3D deep water formation occurs too far south, since it is enhanced with a prescribed salt flux in the Ross and Weddell Seas.”

8. Line 175. What is the ‘TRA minimum’ ?

We changed “TRA minimum” to “temperature minimum in TRA”.

9. Line 212. Is it the southward heat transport?

Yes, we replaced “southward transport” with “southward heat transport”.

10. Line 219. Why is there a difference of one order of magnitude in the results while the difference in the forcing is only a factor 3?

We now added:

“The redistribution heat transport could also be smaller in our case because atmospheric processes are better represented in GCMs (general circulation models), such as the GFDL model used in Winton et al. (2013). The hydrological cycle of the Bern3D EMIC model reacts too weakly compared to another GCM, CESM version 1.0.1, for an ensemble member over the past millennium. Here the Bern3D SSS anomalies were an order of magnitude too low, although showing the same qualitative patterns.”

11. Why is it surprising ?

This could refer either to “surprising” in line 288 or to “surprisingly” in line 309. Line 288 addresses 2000 CE:

“It is surprising that in the Pacific (excluding the SO sector), the same qualitative water mass

anomalies as in 1750 are still present, however displaced northwards, and opposite (...)”

This is different than what we saw in the Atlantic and SO, but may not be surprising indeed. We reformulated this to:

“In the Pacific (excluding the SO sector), the same qualitative water mass anomalies as in 1750 are still present, however displaced northwards. This slower water mass renewal is due to the longer residence time of waters in the Pacific. Opposite (...)”

Line 309 (which is now moved to the appendix; see general comment #1):

“Surprisingly, the change in absolute overturning rate, which is estimated via water age, has practically no influence in all cases except the Atlantic in 2000 CE.”

is now changed to:

“The change in absolute overturning rate, which is estimated via water age, has practically no influence in all cases except the Atlantic in 2000 CE, where the largest overturning anomalies take place.”

12. Line 356. 600 CE is usually not associated with a medieval warm period. The classical ‘Medieval Climate Anomaly’ is rather around 850-1150 CE.

We agree that the MCA or medieval warm period is usually defined later than 600 CE, but we followed Gebbie and Huybers (2019) (GH19 hereafter) such that we can compare our results with theirs. Figure 1a of GH19 shows a warm period (i.e. global average warmer than 0 CE) from ca. 0 to 1200 CE with the maximum temperature in the middle, at 600 CE. Note that this line is now reformulated due to specific comment #17.

13. Line 357 and below (e.g. 364-365). The results of GH19 seems to be well in agreement with the observations. I think this should be mentioned more explicitly and discussed.

We made a few changes around these lines and emphasized that the model of GH19 corresponds well with measured water ages. We have the opinion though that both models have their strengths and weaknesses (static circulation in model of GH19 as measured during transient (early) industrial warming; less realistic circulation/ventilation rates in Bern3D) and none of them represents the truth.

14. Line 369-370. This model bias provides very important information. For me, this has to be explained earlier in order to analyze the implications for all the diagnostics presented.

“(…) because the deep North Atlantic is too old in the Bern3D ocean model compared to radiocarbon observations (Gebbie and Huybers, 2012) (...) These observations show radiocarbon ages of up to 600 years in the North Atlantic (zonal average), whereas we find ideal ages over 900 years (Fig. 8).”

We analyzed the impact of this model bias in more detail and found that it has a smaller impact than we expected. We mention this now briefly in the discussion instead and give more details here: We considered a sensitivity simulation with a smaller bias in North Atlantic water age to see if the deep Atlantic would then be already warming at present, as in GH19. Namely, the maximum age of Atlantic water in OcFIX_strongmix is ca. 800 yr (Fig. R1d) instead of 1000 yr for STD. Although still too old, this compares better to the observations. Since the downward temperature propagation for strongmix (Fig. R2) is very comparable to STD (Fig. 4a, b), we conclude that this model bias is likely not responsible for the differences in downward propagation seen between GH19 and our study.

15. Figure 11. It is not easy to compare with the Figure 2 of GH2019. Could it be possible to reproduce for instance on figure 11 the anomalies deduced from observations (or the results of GH2019 if publicly available) ?

We agree with the reviewer and added a third panel to Fig. 11 with the model results of GH19, Fig. 2. We thank G. Gebbie for providing the data and details on the analysis.

16. Line 377. Is it ‘already warming’ or ‘warmer conditions than in 1875’ ?

‘Warmer conditions than in 1875’ is indeed more correct. We clarified in lines 374-379 that Fig. 11 only shows warming/cooling trends between 1875 and 1995 CE.

17. Line 385. As the model is fast, would it be possible to make an additional experiment to prove this hypothesis ?

We did so and rejected this hypothesis. We now mention in the text instead that including a medieval warm period (MWP) does not alter our main results and provide Fig. R3 and Fig. A6. We performed a coupled simulation OcAtmTRALong starting at 0 CE with a MWP. For consistency

with the later simple evolution, the MWP radiative forcing from 0 to 1200 CE is chosen triangular-shaped with a maximum of 0.35 Wm^{-2} at 600 CE. From 1200 CE the forcing is identical to the forcing in Fig. 1a. OcAtmTRALong supplied the SST, SSS and sea ice boundary conditions for the ocean-only simulations with MWP: OcTRALong and OcFIXLong. We reproduced Fig. 11 now for these runs in Fig. R3. The cooling in the North Pacific in Fig. R3 did not become as strong as in GH19 (i.e., not crossing the -5 cK contour line), which disproves the hypothesis in L385. For completion we also reproduce Fig. 4a, b for OcTRALong and OcFIXLong in Fig. A6 (note the different time axis). These figures are very similar from ca. 1600 CE onward with the notable difference that the cooling in the Pacific does not reach below 2 km anymore for OcFIXLong (in the case of OcFIX the cooling here was less than 5 cK).

18. Line 413. For me, with the experimental design, SSTs are the same but the heat uptake can be different (as circulation for instance can be different).

“In this paper, we held ocean-atmosphere feedbacks and total ocean heat uptake identical between transient and fixed simulations, by prescribing the same SST and SSS time series.”

That is correct and visible in Fig. 7a, which shows different OHC anomalies for OcTRA (total; black line) and OcFIX (changing SST; blue part). We do not mention total ocean heat uptake/content anymore in L413 and L419. We also corrected L43 from “we cannot quantify differences in global ocean heat uptake” to “we cannot quantify differences in global ocean heat uptake that arise from different ocean-atmosphere interactions”. In Fig. 6 and 7 we do actually quantify OHC changes, which in our case differ between TRA and FIX only because of ocean circulation changes. Our ocean-only setup is as if the atmosphere would be an infinite source of heat/cold that provides the heat/cold needed to overwrite the temperature in the surface layer to the desired imposed SST. The amount needed differs between OcTRA and OcFIX because of circulation changes, which determine how much heat/cold is transported down from the surface layer. Evidently, in OcTRA more heat/cold enters the ocean than in OcFIX (see, e.g., Fig. 7a and the larger TRA amplitudes in Fig. 4d).

Anonymous Reviewer #2

Received and published: 3 August 2020

This paper analyzes the effect of ocean circulation changes on the transfer of surface temperature anomalies to the deep ocean on time scales of centuries to millennia. It is motivated by an earlier study of Gebbie and Huybers [Gebbie and Huybers (2019)], which was based on a model with constant ocean circulation as inferred from modern observations by inversion. This is an important question for understanding deep ocean climate evolution, but has also consequences beyond that, for example, how important is this history for the initialization of “historical” simulations. Scheen and Stocker apply first a coupled model of intermediate complexity under idealized radiative forcing to derive surface conditions that mimic the transition to and from the Little Ice Age towards modern global warming and beyond. Then they run ocean-only experiments driven by the surface conditions from the coupled model discriminating between simulations with fixed circulation and free currents. The experimental set-up is well designed and illustrates the long-term behavior of temperature trends at depth in the deep ocean. They find that circulation changes do play a role and may lead to quite different results from GH19. The authors provide some sensitivity studies to explore parameter uncertainty. Thus the tools are quite adequate and they are used in a clever and novel way. The manuscript is written concisely and brings the message across. The abstract provides a good summary. The material and figures are illustrative to support the hypothesis. I find the paper quite convincing but suggest that the authors discuss a bit more the possible shortcomings of their approach. In conclusion, I recommend to accept the manuscript after minor revisions.

We thank the reviewer for this positive evaluation and for the concise summary. We now mention the implication for the initialization of historical simulations in the text. In addition to the points addressed below, we now also discuss another shortcoming in more detail, see #10 of reviewer #1.

General comments

1. The authors describe that the coupled model is run to equilibrium and then the ocean only model is run “using steady state SST and SSS”. Are there other drivers of the ocean model, e.g. momentum flux from the coupled model, or are winds and /or other fluxes prescribed externally?

The Bern3D model is forced with a seasonally varying wind field climatology at the sea surface, which is unchanged throughout simulations. The wind field is identical for coupled and ocean-only simulations. We now added this in the text.

There are no other drivers, except for sea ice, which was already mentioned in the text. In the coupled model, sea ice is dynamically simulated where the atmospheric temperature is cold enough. Since diagnosing atmospheric temperature is not possible for ocean-only, a time-varying sea ice area was implemented as boundary condition (from OcAtmTRA; together with SST and SSS).

2. If I understand correctly, the authors can in this set-up only study the effect of density changes on the circulation and the resulting feedback on temperature and salinity transfers. But in the “real” world of the last millennium, for example strong volcanic eruptions may have changed the dynamics of ocean and atmosphere for decades to centuries. It should be mentioned that such effects are not included here.

Long-term effects of volcanic forcing are implicitly included in the LIA segment of the total radiative forcing we use. Pulse-like volcanic coolings are not considered, since we excluded decadal oscillations on purpose in our idealized forcing in order to obtain a clean and less complex signal of downward temperature propagation of longer cold and warm spells. We already mention in L77:

“Possible radiative forcings due to land-use change, volcanic eruptions or solar irradiation are not considered in our illustrative scenario.”

3. How different are the circulation and simulated features in the coupled simulation, compared to the ocean stand-alone run? Is the AMOC or meridional heat transport history similar? A large part of the finding depends on the history of the AMOC in the model.

The evolution of MOC during the coupled runs is given in Fig. R4. These time series are very similar to the ocean-only situation (Fig. 2) except that they start at different steady state values. The difference between the coupled and ocean-only situation in steady state is as described in line 115-119:

“During the extended spin-up, adjustments of the global ocean circulation take place: the steady state Atlantic meridional overturning circulation (AMOC) maximum decreases by 1.5 Sv and the strength of the global meridional overturning circulation (MOC) decreases by 0.8 Sv. Deep ocean temperatures are 0.3 to 0.6°C colder below 3 km, because of a relative increase of Antarctic Bottom Water (AABW) with respect to North Atlantic Deep Water (NADW), and are up to 0.2°C warmer in the depth range from 500 to 3000 m due to an absolute decrease in NADW.”

4. The AMOC slightly strengthens during the LIA cooling and then weakens under modern warming. Does this mean that the cooling/warming drives the AMOC in this model? One could also assume that the cold surface conditions in the LIA North Atlantic were a result of weak AMOC and slow heat transports as has been put forward by many authors. Would the findings of this study still hold?

The cooling/warming seems to be mainly driving the AMOC in our simulations, but it goes both ways since we also observed a warming hole in the North Atlantic SST caused by the AMOC response (not shown). If the AMOC would slow down more and drive more SST changes, possibly the results would be more like Winton et al. (2013), who find an even stronger redistribution heat transport (although other differences between the set-ups and GFDL vs. Bern3D exist).

5. It is said that “simulations with fixed ocean circulation are implemented by using diagnosed values at every grid-point from the steady state”. Which variables are used, only horizontal velocities, or also diffusion/mixing coefficients?

Only the density is saved for every time step during 1 simulation year. The velocities in x-, y- and z-direction follow from frictional geostrophic and hydrostatic balance, which in turn determine the transport of temperature and salinity by advection, diffusion and convection. We added this briefly in the text.

All 3 diffusion/mixing coefficients of the Bern3D ocean (isopycnal, diapycnal and Gent-McWilliams diffusivity) are globally uniform and stay constant throughout the simulations for both TRA and FIX. Note that diapycnal diffusivity was varied in the sensitivity studies.

Minor issues

1. Ln 73: :idealized forcing: was the forcing tuned in this way to get the desired SST time series to be similar to GH19 or is it based on estimates how the radiative forcing actually changed?

We added:

“The forcing was chosen to get a global average SST time series that is comparable to Gebbie and Huybers (2019).”

2. Ln 107: “at every grid cell are set to a latitude-longitude field”: this is very unclear.
Reformulated, see specific comment #2 of reviewer 1.
3. Ln 219: Was the Winton experiment a 1% CO₂ increase per year experiment?
Yes. This information is now added in the text.
4. Ln 221: should be: “column integrated heat content per unit area”
Done, thank you. We also changed the synonym “ocean heat density (OHD)” to “ocean heat areal density (OHD)”.

References

- Gebbie, G. and Huybers, P.: The Mean Age of Ocean Waters Inferred from Radiocarbon Observations: Sensitivity to Surface Sources and Accounting for Mixing Histories, *Journal of Physical Oceanography*, 42, 291–305, <https://doi.org/10.1175/JPO-D-11-043.1>, 2012.
- Gebbie, G. and Huybers, P.: The Little Ice Age and 20th-century deep Pacific cooling, *Science*, 363, 70–74, <https://doi.org/10.1126/science.aar8413>, 2019.
- Moffa-Sánchez, P., Moreno-Chamarro, E., Reynolds, D. J., Ortega, P., Cunningham, L., Swingedouw, D., Amrhein, D. E., Halfar, J., Jonkers, L., Jungclaus, J. H., Perner, K., Wanamaker, A., and Yeager, S.: Variability in the Northern North Atlantic and Arctic Oceans Across the Last Two Millennia: A Review, *Paleoceanography and Paleoclimatology*, 34, 1399–1436, <https://doi.org/10.1029/2018PA003508>, 2019.
- Winton, M., Griffies, S. M., Samuels, B. L., Sarmiento, J. L., and Frölicher, T. L.: Connecting Changing Ocean Circulation with Changing Climate, *Journal of Climate*, 26, 2268–2278, <https://doi.org/10.1175/JCLI-D-12-00296.1>, 2013.

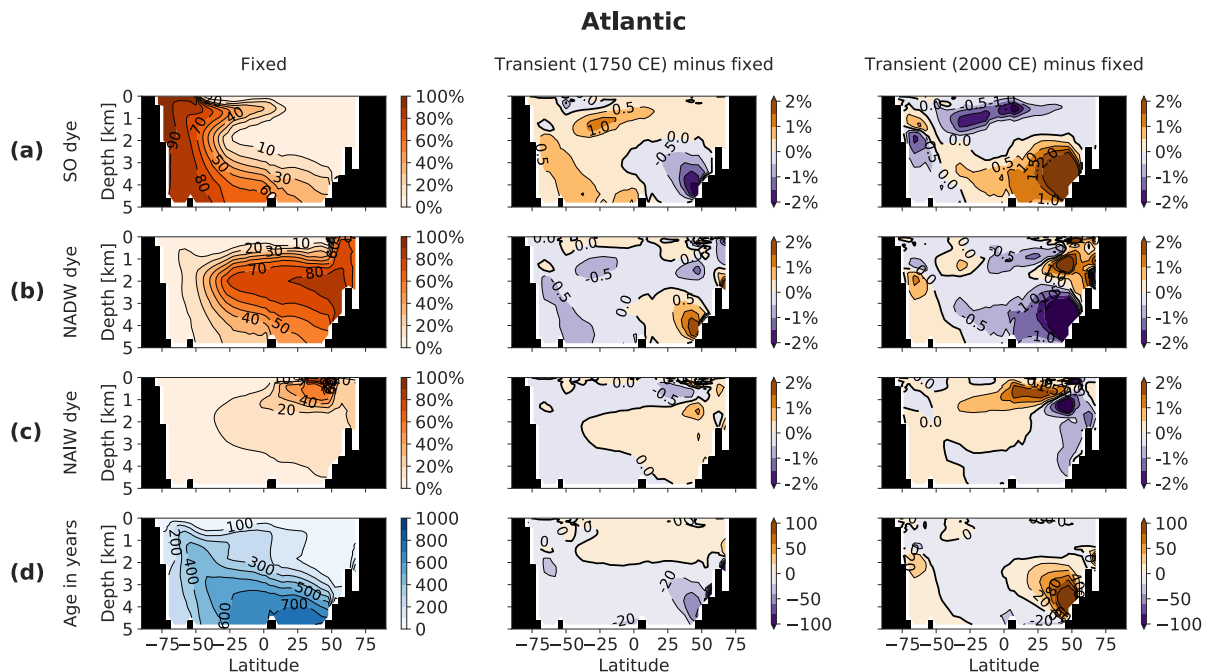


Figure 1: For specific comment #14 of reviewer #1: reproduction of Fig. 8 (see caption there), now for runs OcTRA_strongmix and OcFIX_strongmix.

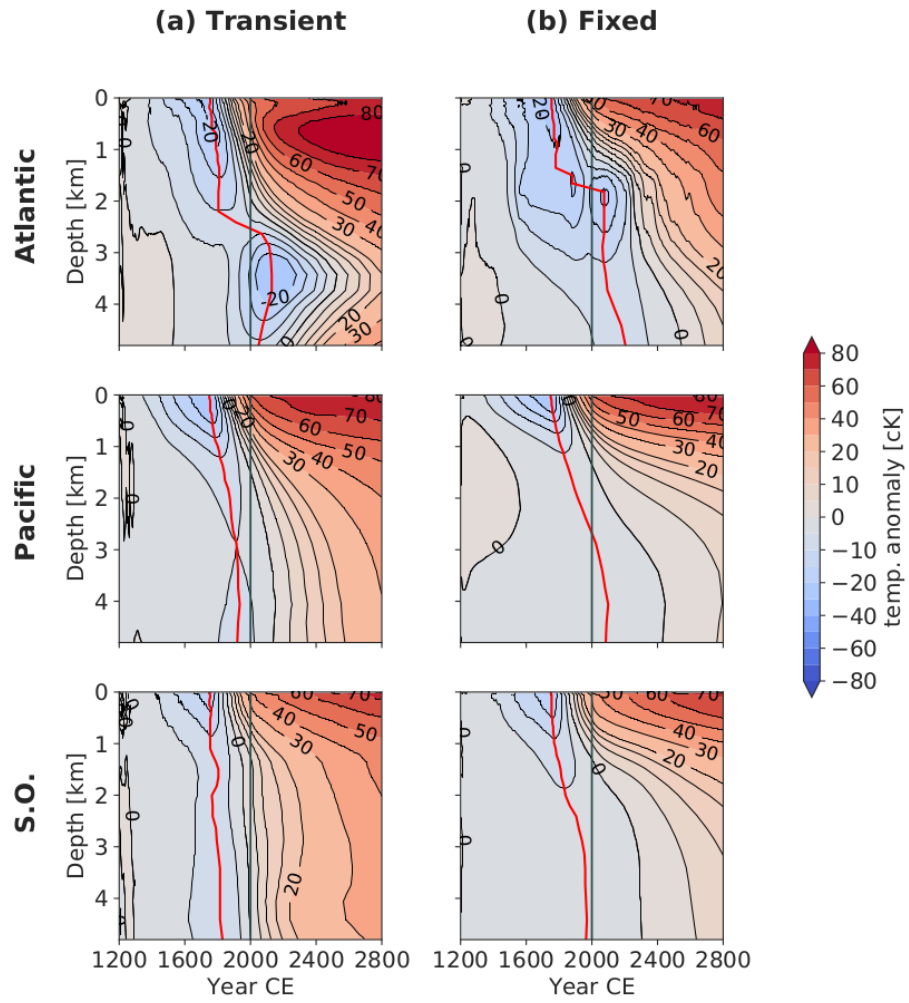


Figure 2: For specific comment #14 of reviewer #1: reproduction of Fig. 4a, b (see caption there), now for runs OcTRA_strongmix and OcFIX_strongmix.

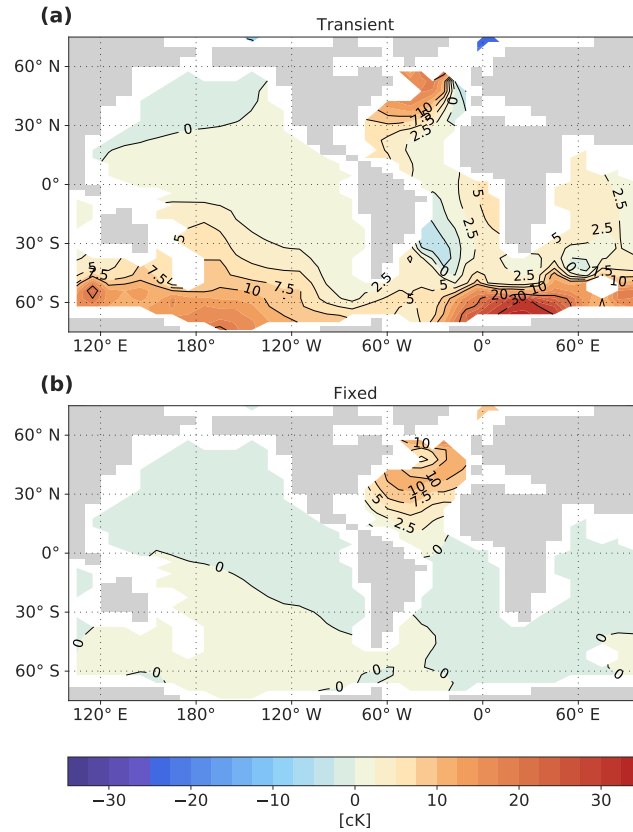


Figure 3: For specific comment #17 of reviewer #1: reproduction of Fig. 11 (see caption there), now for runs OcTRALong and OcFIXLong, which include a medieval warm period between 0 and 1200 CE and from 1200 to 2800 CE have forcing identical to STD.

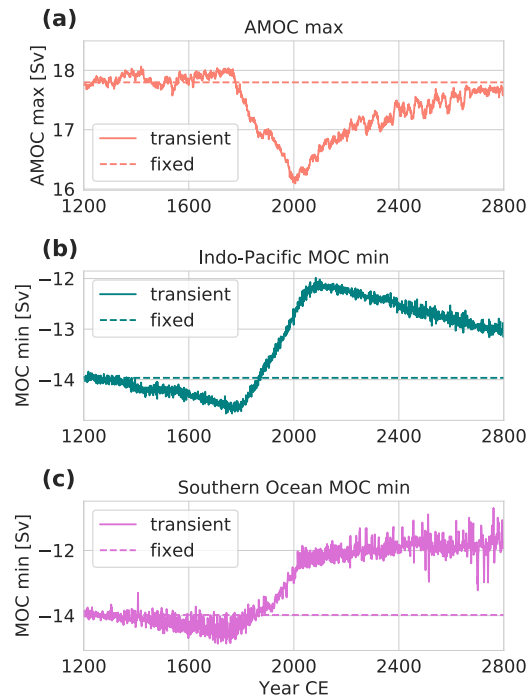


Figure 4: For general comment #3 of reviewer #2: reproduction of Fig. 2 (see caption there), now for the coupled runs OcAtmTRA and OcAtmFIX.

Effect of changing ocean circulation on deep ocean temperature in the last millennium

Jeemijn Scheen^{1,2} and Thomas F. Stocker^{1,2}

¹Climate and Environmental Physics, Physics Institute, University of Bern, Bern, Switzerland

²Oeschger Centre for Climate Change Research, University of Bern, Bern, Switzerland

Correspondence: Jeemijn Scheen (jeemijn.scheen@climate.unibe.ch)

Abstract. Paleoreconstructions and modern observations provide us with anomalies of surface temperature over the past millennium. The history of deep ocean temperatures is much less well-known and was simulated in a recent study for the past 2000 years under forced surface temperature anomalies [and fixed ocean circulation](#). In this study, we simulate the past 800 years with an illustrative forcing scenario in the Bern3D ocean model, which enables us to assess the role of changes in ocean circulation on deep ocean temperature. We quantify the effect of changing ocean circulation by comparing transient simulations (where the ocean dynamically adjusts to anomalies in surface temperature – hence density) to simulations with fixed ocean circulation. We decompose temperature, ocean heat content and meridional heat transport into the contributions from changing ocean circulation and changing sea surface temperature (SST). In the deep ocean, the contribution from changing ocean circulation is found to be as important as the changing SST signal itself. Firstly, the small changes in ocean circulation amplify the Little Ice Age signal around 3 km depth by at least a factor of two, depending on the basin. Secondly, they fasten the arrival of this atmospheric signal in the Pacific and Southern Ocean at all depths, whereas they delay the arrival in the Atlantic between about 2.5 and 3.5 km by two centuries. This delay is explained by an initial competition between the Little Ice Age cooling and a warming due to an increase in relatively warmer North Atlantic Deep Water at the cost of Antarctic Bottom Water. Under the consecutive AMOC slowdown, this shift in water masses is inverted and aging of the water causes a late additional cooling. Our results suggest that small changes in ocean circulation can have a large impact on the amplitude and timing of ocean temperature anomalies below 2 km depth.

1 Introduction

The climate period from 1200 to 1750 CE manifests modes of natural variability and response to solar and volcanic forcing without the substantial anthropogenic radiative forcing from increased greenhouse gas concentrations (Masson-Delmotte et al., 2013). A growing paleoclimatic database of surface reconstructions exists that quantifies this natural variability with at least continental resolution (Mann et al. (1998, 2009); McGregor et al. (2015); Neukom et al. (2019); PAGES 2k Consortium: PAGES 2k Consortium (2013) and Emile-Geay et al. (2017)). Early instrumental records, based on surface measurements and their combination with models, permit the separation of climate responses due to solar and volcanic forcing respectively (Brönnimann et al., 2019), but oceanic reconstructions below the sea surface are ~~much scarcer, especially in the deep ocean~~

25 ([Abraham et al., 2013](#); [Levin et al., 2019](#)). For example, only 17% of the ocean cores used in [McGregor et al. \(2015\)](#) lie below 2000 and only 2% below 3000. [scarce for the last millennium \(Moffa-Sánchez et al., 2019\)](#). Therefore, models can be of great value by simulating past and present deep ocean temperatures in agreement with paleoclimatic reconstructions at the surface.

This study focuses on the propagation of atmospheric temperature anomalies into the deep ocean and is motivated by [Gebbie and Huybers \(2019\)](#), who investigated this during the past 2000 years. They used an ocean model with fixed circulation, which they inferred from modern observations and constrained by measurements of the legendary HMS *Challenger* expedition of 1872-1876. The changes they found in deep ocean temperature in the Atlantic and Pacific are delayed responses to variations of the forced surface climate. We wonder to what extent their results would be different with a model that [exhibits dynamically changing circulation](#) [permits a dynamical response of the circulation to the forcing](#). In this study, we test this with the Bern3D model.

35 Previous studies have pointed out that temperature cannot always be approximated as a passive tracer, since it induces circulation changes, which influence the patterns of heat uptake ([Banks and Gregory, 2006](#); [Xie and Vallis, 2011](#); [Winton et al., 2013](#); [Marshall et al., 2015](#); [Garuba and Klinger, 2016](#)). These authors used various approaches to separate the effects of changing circulation (also called redistribution transport) and changing sea surface temperature (SST). [Banks and Gregory \(2006\)](#), [Marshall et al. \(2015\)](#) and [Garuba and Klinger \(2016\)](#) used a passive tracer that diagnoses the effect of changing SST only, whereas [Xie and Vallis \(2011\)](#) used a tracer diagnosing the effect of changing circulation only, and [Winton et al. \(2013\)](#) ran simulations with artificially fixed (FIX) ocean circulation in addition to transient (TRA) simulations with dynamically changing circulation. Here we follow the latter approach, although with ocean-only simulations in order to make sure that fixed and transient simulations undergo the exact same surface boundary conditions. By prescribing these SST and sea surface salinity (SSS) fields, we cannot quantify differences in global ocean heat uptake [anymore that arise from different ocean-atmosphere interactions](#), as was done in [Winton et al. \(2013\)](#). In exchange, this allows us to quantify the downward propagation of small temperature anomalies to the abyss and the spatial pattern of heat uptake without biases due to ocean-atmosphere feedbacks, which differ between transient and fixed simulations.

The paper is organized as follows. Section 2 presents the model and the methods needed to disentangle surface signal changes from those caused by circulation changes. In Sect. 3, we analyse the propagation of temperature signals into the deep ocean and decompose them according to different physical mechanisms. Section 4 investigates the causes of leads and lags registered at depth in the different ocean basins, including their sensitivity on changes in mixing and wind stress. In Sect. 5, we [critically](#) compare our results with the study of [Gebbie and Huybers \(2019\)](#) and [we](#) conclude in Sect. 6.

2 Modelling framework

2.1 Model description

55 We use an Earth system Model of Intermediate Complexity (EMIC), the Bern3D model version 2.0, developed by [Ritz et al. \(2011\)](#) and systematically constrained by observations ([Roth et al., 2014](#)). The model consists of a 3-dimensional dynamic ocean circulation model with 32 depth layers coupled to a 1-layer atmosphere and a land biosphere. The ocean component of

the model is based on frictional geostrophic balance equations (Edwards et al., 1998; Müller et al., 2006), and the atmosphere consists of an energy balance model including a parametrized hydrological cycle (Ritz et al., 2011). The Bern3D has an equilibrium climate sensitivity of 3.0°C in the standard version. Seasonally varying winds are added as a fixed forcing. Sea-ice growth and melt are thermodynamically simulated. The horizontal grid resolution is 40×41 cells, and the time step is 3.8 days (Roth et al. (2014), Appendix A). Because of its relatively coarse resolution and reduced complexity in the atmosphere, the model is well suited for long simulations and sensitivity studies. For example, 5,000 model years can be simulated within 24 hours.

Here, we use the idealized age tracer, which provides information about changes in the absolute strength of the circulation, and a number of dye tracers to identify relative changes in water masses. The idealized ocean age tracer (England, 1995; Hall and Haine, 2002) records the time since water was last in contact with the atmosphere. It satisfies the transport equation like any other conservative tracer implemented in the ocean model with the additional production term 1 yr yr^{-1} . When water reaches the surface, the ideal age is reset to zero. Dye tracers track the water that originates from a certain surface area of the ocean, e.g., the Southern Ocean (Fig. A1). At the surface we restore the tracer concentration to the value 100 % in the area of origin of the specific dye tracer, and 0 % elsewhere. Restoring is not instantaneous, but occurs on a time scale of 20 days in order to avoid numerical problems. Ideal age and dye tracers are spun up simultaneously with the circulation such that they are at their equilibrium distribution at the start of the experiments.

2.2 Radiative forcing of medieval cooling and early industrial warming

We simulate the past 800 years followed by 800 years in the future, using an idealized radiative forcing (Fig. 1a). Simulations start from a pre-industrial steady state at 1200 CE. The amplitudes of the medieval cooling (1200-1750 CE), also referred to as Little Ice Age (LIA), and the subsequent industrial warming (1750-2000 CE) are followed by 800 years of constant radiative forcing. Our illustrative scenario represents this by a linear decrease in radiative forcing by -0.55 Wm^{-2} over 1200-1750 CE followed by an increase to $+1.4 \text{ Wm}^{-2}$ from 1750 to 2000 and constant thereafter. [The forcing was chosen to get a global average SST time series that is comparable to Gebbie and Huybers \(2019\)](#). Possible radiative forcings due to land-use change, volcanic eruptions or solar irradiation are not considered in our illustrative scenario.

While the exact radiative forcing is of lesser relevance here, we note that the global average SST anomalies are comparable with reconstructions (PAGES 2k Consortium, 2013; Rayner et al., 2003). Our global SST anomaly shows a cooling amplitude of -0.24 K followed by a $+0.74 \text{ K}$ warming until 2000 CE (Fig. 1b) and approximately follows the SST variations reported by Gebbie and Huybers (2019) (-0.27 K ; $+0.87 \text{ K}$; from their Fig. 1a), which are in turn based on proxy reconstructions from the PAGES 2k Consortium (PAGES 2k Consortium, 2013) before 1950 CE and instrumental data from HadISST after 1870 CE (Rayner et al., 2003). For the overlap period (1870-1950), Gebbie and Huybers (2019) take a weighted linear combination of the two such that their resulting warming amplitude ($+0.87 \text{ K}$) is higher than the proxy-only signal (PAGES 2k Consortium (2013): $+0.53\text{K}$), because the instrumental data exhibit a larger amplitude of industrial warming.

Table 1. Simulations performed in this study.

Simulation	Model ^a	Ocean ^b	Parameters ^c	Notes
OcAtmTRA	coupled	transient	-	generates SST/SSS/sea ice area fields each time step
<u>OcAtmFIX</u>	<u>coupled</u>	<u>fixed</u>	<u>-</u>	<u>not shown</u>
OcTRA	ocean	transient	-	standard simulation
OcFIX	ocean	fixed	-	standard simulation
OcTRA_weakmix	ocean	transient	$K_D \times \frac{1}{2}$	
OcFIX_weakmix	ocean	fixed	$K_D \times \frac{1}{2}$	
OcTRA_strongmix	ocean	transient	$K_D \times 2$	
OcFIX_strongmix	ocean	fixed	$K_D \times 2$	
OcTRA_weakwind	ocean	transient	$\tau_{wind} \times \frac{1}{2}$	
OcFIX_weakwind	ocean	fixed	$\tau_{wind} \times \frac{1}{2}$	
OcTRA_strongwind	ocean	transient	$\tau_{wind} \times 2$	
OcFIX_strongwind	ocean	fixed	$\tau_{wind} \times 2$	
<u>OcAtmTRALong</u>	<u>coupled</u>	<u>transient</u>	<u>-</u>	<u>provides SST/SSS/sea ice for OcTRALong, OcFIXLong</u>
<u>OcTRALong</u>	<u>ocean</u>	<u>transient</u>	<u>-</u>	<u>extended run (0–2800 CE) with medieval warm period</u>
<u>OcFIXLong</u>	<u>ocean</u>	<u>fixed</u>	<u>-</u>	<u>extended run (0–2800 CE) with medieval warm period</u>

^a Simulations are either run using the coupled Bern3D (with radiative forcing in the atmosphere as in Fig. 1a) or as ocean-only Bern3D (prescribed SST, SSS and sea ice from OcAtmTRA).

^b Ocean circulation can be fixed or transient, i.e., responding to SST and SSS changes.

^c In sensitivity simulations, the mixing parameter K_D (diapycnal diffusivity) and wind stress τ_{wind} are varied.

90 2.3 Simulations with fixed and transient ocean circulation

Quantification of the influence of changing ocean circulation on the tracer distributions of temperature and salinity is not trivial, because temperature and salinity are ‘active’ tracers, which influence the ocean circulation through changes in density. We disentangle the effects caused by changes in the surface values from those caused by circulation changes by requiring for every experiment two simulations: one in which the ocean circulation adjusts transiently to the buoyancy distribution and one
95 in which the circulation is kept constant, both forced with identical surface boundary conditions.

Simulations with fixed ocean circulation are implemented by using diagnosed values of the density at every grid cell from one annual cycle at steady state. The velocities in x-, y- and z-direction follow from frictional geostrophic and hydrostatic balance. Therefore, the circulation, including advection, diffusion and convection, is maintaining a perpetual seasonal cycle and does not respond to SST changes impacted by atmospheric changes at the ocean surface. Note that unphysical effects
100 could arise, e.g., when convection still operates, although the water column at that location could now be stably stratified. This

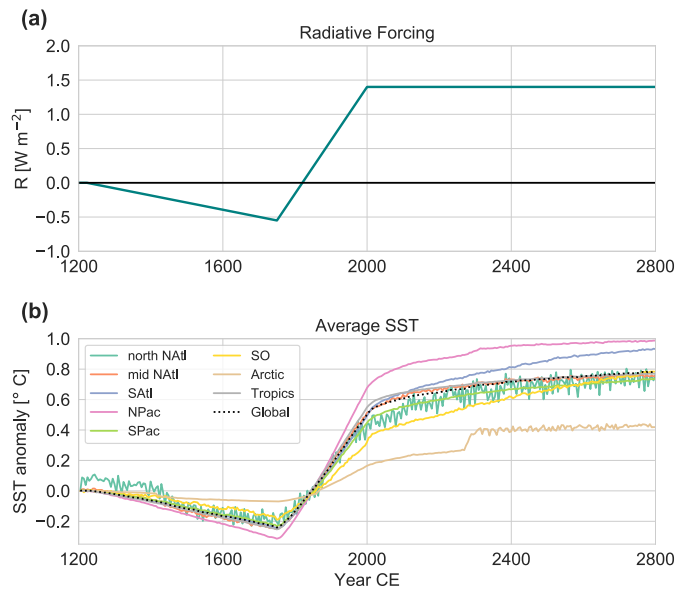


Figure 1. (a) Idealized radiative forcing, which is used in the case of coupled simulations (OcAtmTRA and OcAtmFIX, see Table 1). (b) Sea surface temperature anomaly as a result of the forcing in (a): globally (black, dotted line) and averaged per region (colors, defined in Fig. A1). The global average SST at 1200 CE is 18.0°C .

approach allows us to isolate the effect of changing ocean circulation by taking the difference between a transient and a fixed run under the same boundary conditions. This is realized by a series of ocean-only simulation pairs, summarized in Table 1.

Crucial to our approach is that these boundary conditions must be identical at the atmosphere-ocean interface and not, e.g., at the top of the atmosphere. When we use the fully coupled Bern3D with transient ocean circulation (OcAtmTRA) and with fixed circulation (OcAtmFIX; not used elsewhere) under the same radiative forcing, the resulting two simulations possess different SST and SSS patterns, because ocean-atmosphere feedbacks differ between the transient and fixed case, as was already suggested by Garuba and Klinger (2016). These SST differences are small, but of the same order of magnitude as the changes in deep ocean temperature, and would therefore mask the signal we want to detect. We resolve this by running the model in an ocean-only mode that is forced with the same SST, SSS and sea ice in both transient and fixed simulations. The possibility to run the Bern3D model under time-varying surface boundary conditions has been newly implemented for this study. For every time step of the 1600 simulation years, the SST, SSS and sea ice ~~at every surface grid cell of surface grid cells~~ are set to ~~a latitude-longitude field that is the corresponding value in the (latitude, longitude, time step) boundary conditions that are~~ obtained from a previous coupled transient simulation OcAtmTRA over 1600 years (Fig. 1). All ocean-only simulations in Table 1 are run under identical surface boundary conditions ~~obtained saved~~ from the OcAtmTRA simulation from year 1200 to 2800 CE. ~~The coupled and ocean-only model are forced with the same seasonally varying wind field climatology.~~

2.4 Steady state

The coupled simulations are run to equilibrium under pre-industrial conditions. When switching to the ocean-only configuration, a model drift is observed that requires an extension of the spin-up. The ocean-only model is run for another 5000 years using the steady state SST, SSS and sea ice distributions from a period of 100 years, repeated 50 times. Afterwards, the ocean-
120 only simulations OcTRA and OcFIX are started. During the extended spin-up, adjustments of the global ocean circulation take place: the steady state Atlantic meridional overturning circulation (AMOC) maximum decreases by 1.5 Sv and the strength of the global meridional overturning circulation (MOC) decreases by 0.8 Sv. Deep ocean temperatures are 0.3 to 0.6°C colder below 3 km, because of a relative increase of Antarctic Bottom Water (AABW) with respect to North Atlantic Deep Water (NADW), and are up to 0.2°C warmer in the depth range from 500 to 3000 m due to an absolute decrease in NADW. By the
125 end of this additional spin-up, the residual drift of basin-mean ocean temperature at 3 km depth during the last 500 simulation years is less than $4 \cdot 10^{-6}$ K/yr in the Pacific and less than $2 \cdot 10^{-6}$ K/yr in the Atlantic. ~~Simulations~~ Sensitivity simulations with varying mixing and wind stress require their own steady state. For each of these four simulation pairs, we perform a similar 5000 year ocean-only spin-up, but with the respective parameter values given in Table 1.

3 Results and discussion

130 3.1 Circulation change

Figure 2 shows the responses of the MOCs in the Atlantic (AMOC), the Indo-Pacific (IPMOC) and Southern Ocean (SOMOC) for the ocean-only simulations forced by the imposed surface fields during the 1600 simulation years. Maxima and minima are evaluated below a depth of 400 m in order to avoid shallow Ekman-driven overturning cells. The Atlantic, Pacific and Indian basins are defined between 35°S and up to 70°N, and the Southern Ocean (SO) extends southward of 35°S throughout
135 this study, unless indicated otherwise. By design, the circulation is constant over time in the fixed case. During the medieval cooling, the AMOC slightly increases by ~ 0.2 Sv, whereas the negative IPMOC and SOMOC both strengthen by ~ 0.7 Sv. Industrial warming starting in 1750 causes the AMOC to slow down by 1.5 Sv, whereas both the IPMOC and SOMOC weaken by about ~ 2.2 Sv until 2000. This 1.5 Sv AMOC slowdown is within the 1σ CMIP5 range of fully coupled AOGCMs ~~and the AMOC in that model mean experiences a similar decrease of 2 from 2000 to 2100 CE~~ under low emission forcing (Collins
140 et al., 2019). After 2000, the AMOC maximum recovers under the constant forcing with a relaxation time scale of about 470 yr, whereas the IPMOC takes significantly longer to reach equilibrium, and for this case a well-constrained time scale cannot be determined from the present simulations. The SOMOC does not recover, but weakens by an additional ~ 1.3 Sv over the final 800 years.

The overturning stream functions are shown in Fig. 3 at 1205 CE and their anomalies at years 1750 CE and 2000 CE
145 (simulation OcTRA). The AMOC deepens during the medieval cooling phase, which leads to an increase of about 0.8 Sv at 2 km depth, although the maximum AMOC increased only by ~ 0.2 Sv by 1750 (Fig. 4a). The largest changes of the AMOC occur during the industrial warming at depths of 2 km reaching up to 2 Sv, and the reduction of overturning occupies the

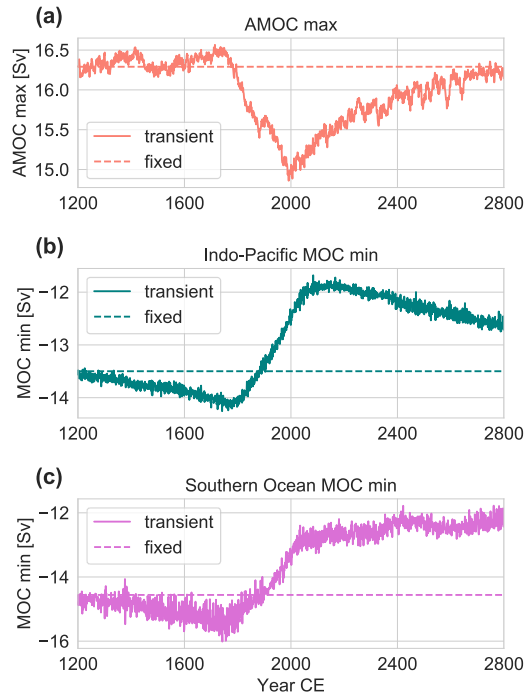


Figure 2. Response of the maximum respectively minimum values of the meridional overturning circulation (MOC) to imposed SST, SSS and sea ice (Fig. 1b). **(a)** Atlantic MOC maximum, **(b)** minimum of the MOC in the combined Pacific and Indian basins (IPMOC) and **(c)** in the Southern Ocean (SOMOC). Simulations OcTRA (transient) and OcFIX (fixed) are shown.

entire Atlantic ocean basin from 1 to 3 km depth. IPMOC changes are primarily located in the southern hemisphere with a strengthening of the circulation below 3 km at the southern margin of the basin during the medieval cooling, and a subsequent
 150 weakening above 3 km. The global MOC shows a strong bipolar response to the medieval cooling and industrial warming. That is, the absolute value of MOC strength increases in both hemispheres from 1205 to 1750, and a subsequent opposite and stronger response is simulated during the industrial warming.

3.2 Propagation of temperature anomalies into the deep ocean

We now turn to the propagation of the atmospheric temperature anomaly into the deep ocean. [Figure 4a](#), [Figures 4a and b](#) show
 155 Hovmöller diagrams illustrating the development of the basin-averaged temperature anomalies as a function of depth for each ocean basin. Temperature anomalies are small and reported here in units of centi-Kelvin ($1 \text{ cK} = 10^{-2} \text{ K}$). The propagation of the LIA cooling into the deep ocean is clearly visible, followed by the industrial warming signal. Qualitatively distinct patterns for the transient (TRA) and fixed (FIX) circulations emerge in all basins with a generally faster and stronger transfer of the anomalies to the deep ocean in the TRA case. However, local differences appear, particularly in the Atlantic Ocean. For TRA,
 160 the deep Atlantic shows an isolated cold anomaly at about 3 km depth, which develops by the end of the medieval cooling

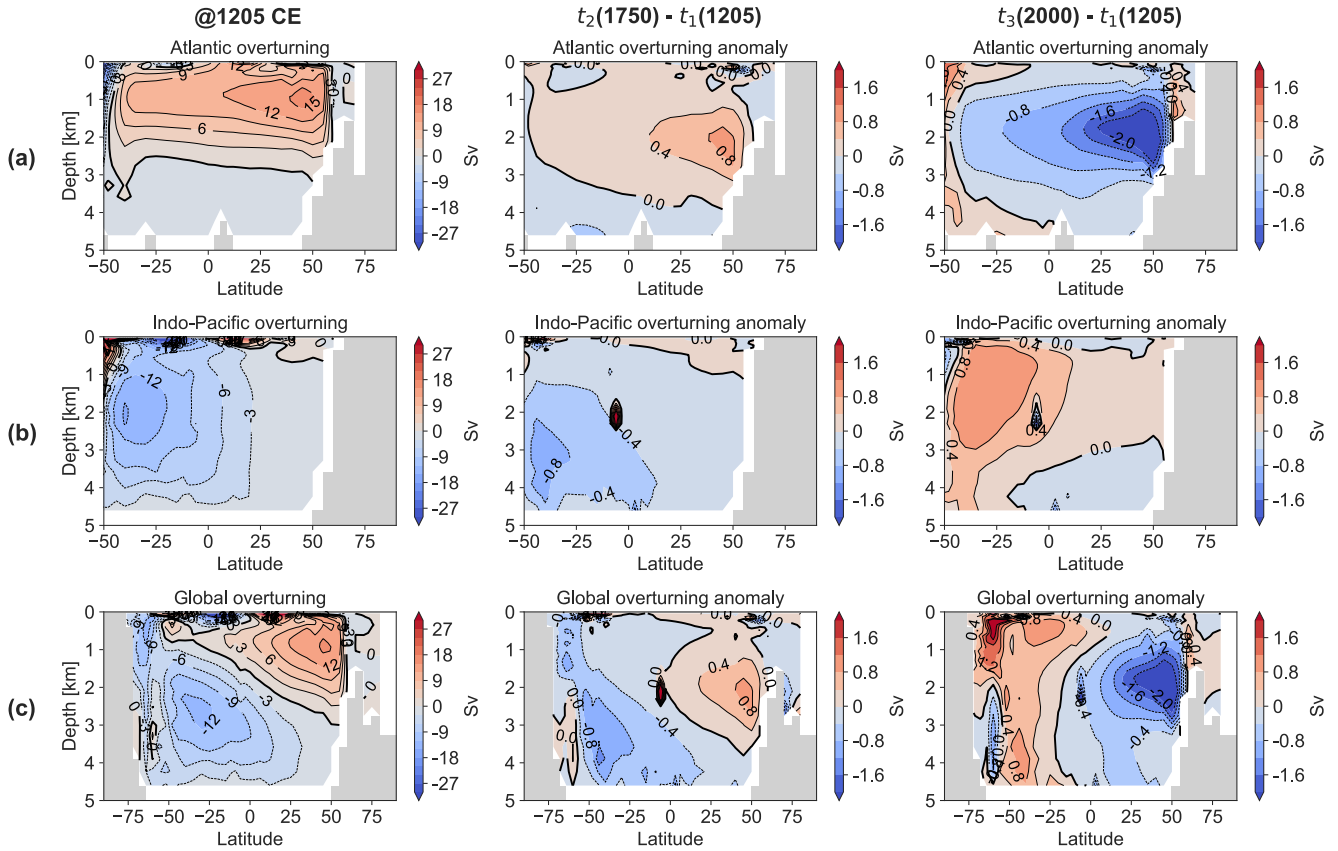


Figure 3. Meridional overturning circulation for the transient ocean-only simulation OcTRA for (a) the Atlantic (AMOC), (b) the Indo-Pacific (IPMOC) and (c) globally at different time steps: at the start (1205 CE) and the anomalies at the coldest point of the Little Ice Age (1750 CE) and in 2000 CE. Values are averages over 15 years (for 1205-1220 CE) respectively 30 years (around 1750 and 2000 CE). Note the changing colorbar and latitude axis. The overturning stream function is positive (red) for water rotating clockwise and negative (blue) for counterclockwise.

period and persists for several centuries. This feature, observed in the more realistic TRA simulation, suggests that the cold anomaly created by the pre-industrial cooling can be detected long into the future. It is evident that this anomaly is a result of the changes in MOC, as the fixed circulation case does not exhibit this isolated anomaly. At year 2000 in TRA, the cooling is still strong and occurs below 2.5 km depth in the Atlantic, whereas for FIX much weaker cooling is confined to below 3 km. On the other hand, in the Pacific basin, where the MOC changes during the warming are generally smaller, the signal propagation into depth is rather uniform and follows the surface forcing with a delay due to ocean circulation. Here, the faster signal transfer to depth in TRA is particularly evident. The SO also shows a uniform signal propagation with a faster transfer in TRA.

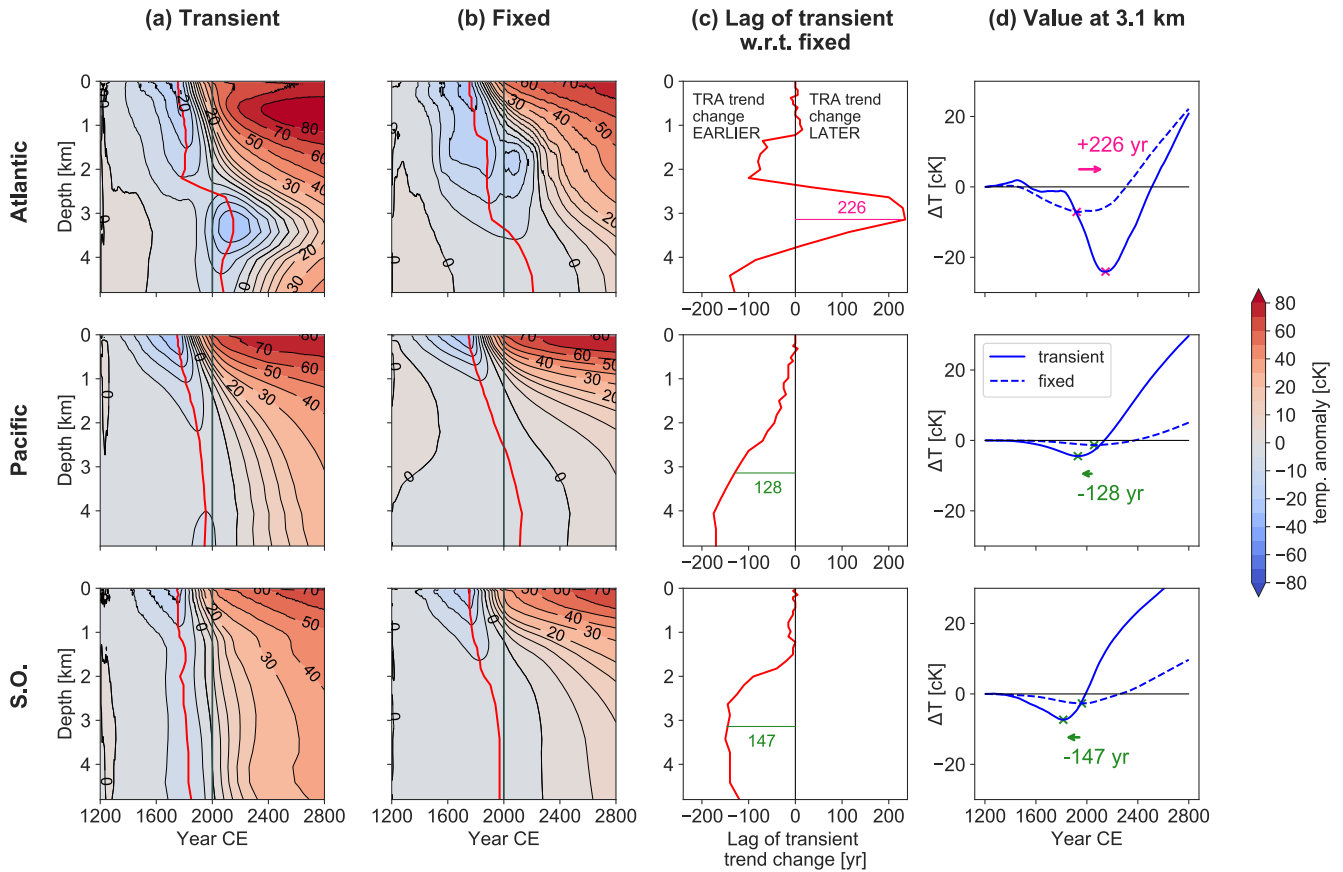


Figure 4. (a), (b) Hovmöller diagrams of temperature anomalies in centi-Kelvin ($1 \text{ cK} = 10^{-2} \text{ K}$) over depth. Values are basin averages of the Atlantic or Pacific (35°S – 70°N) or the Southern Ocean ($< 35^{\circ}\text{S}$), respectively. Colour levels increase in steps of 5 cK from -20 cK to 20 cK and in steps of 10 cK otherwise. Red lines track the minimum temperature anomaly and indicate where the temperature trend changes from cooling to warming. (c) The lag in occurrence of the transient minimum temperature anomaly w.r.t. the fixed. This equals the red line in (a) minus the red line in (b). (d) Temperature anomalies from (a), (b) are repeated for a fixed 3.1 km depth. Pink and green arrows indicate lags (positive) and leads (negative) of the transient w.r.t fixed simulation in the temperature trend change at this depth (also indicated in (c)). Results are for simulations OcTRA (transient) and OcFIX (fixed).

In the Atlantic, the more effective downward propagation of negative temperature anomalies in TRA is linked to water mass changes in the proportion of AABW versus NADW, as AABW water is about 3°C colder than NADW. At the end of the simulation (2800 CE), relatively more cold AABW at the expense of NADW is observed at depths from 2 to 4 km, which corresponds to the location of the persistent cold anomaly. This is illustrated by dye tracers tracking AABW and NADW in Fig. A3). The opposite (an increase in NADW at the expense of AABW) occurs above 2 km and below 4 km, explaining the stronger Atlantic warming in TRA at these depths. In the Pacific, the more effective downward transport in TRA is explained by increased inflow of deep southern water during the cooling and afterwards the positive IPMOC anomaly causes less inflow of cold AABW during the subsequent warming and hence a more effective warming at depth in TRA than in FIX (see Fig. 3). The SO is already warming in year 2000 for both TRA and FIX, because of its high ventilation rate. This ventilation rate in the SO (Fig. 8d, 9d) agrees well with radiocarbon-based observations (Gebbie and Huybers, 2012) in the average and maximum SO water age, although qualitatively the Bern3D deep water formation occurs too far south (since it is enhanced with a prescribed salt flux in the Ross and Weddell Seas).

The red lines in Fig. 4a and b track the minimum temperature anomaly at every depth. This helps us identify whether the deep ocean at present (2000 CE) is still cooling (red line to the right of vertical line), or already warming. Leads and lags of the temperature minimum of the two simulations FIX and TRA can be readily determined. Figure 4c provides the depth dependence of the lag of the temperature minimum in TRA with respect to that in FIX. The TRA minimum in temperature minimum in TRA in the Pacific and the SO appears earlier and this lead grows up to 150 years at depth. In the Atlantic, this structure is interrupted by a strong lag between 2.5 and 4 km of over 200 years. Hence, changing circulation accelerates the propagation of the downward signal everywhere except in the Atlantic between 2.5 and 3.5 km depth, providing a mechanism for ocean memory of past changes in surface climate. In Sect. 4, we will carry out sensitivity tests to assess the robustness of our findings.

Figure 4d presents the time series view of temperature anomalies at 3.1 km, the depth where the strongest differences between the basins are found. Here, changes in ocean circulation delay the arrival of industrial warming by more than 200 years in the deep Atlantic, whereas they accelerate the arrival by about 120 and 150 years in the deep Pacific and deep SO, respectively. Another notable feature is that the amplitude is higher for TRA than for FIX in each basin. As discussed in Sect. 4, this is a robust feature. Similarly, Xie and Vallis (2011) found that changing ocean circulation increases the effective depth to which anomalous heat reaches under their warming experiments. They attribute this to changing circulation allowing for more heat uptake via a) reducing average SST and b) reducing surface heat loss at high latitudes. ~~As both explanations involve SST differences between OeTRA and OeFIX, which we do not have in our set-up, there must be even more reasons why circulation changes promote the downward propagation of temperature anomalies.~~

3.3 Decomposition of temperature anomalies

200 Anomalies of the transport of a quantity $Q = Q(x, y, z)$, $v Q$, in the ocean can be decomposed into contributions originating from changes in transport velocity v and in the quantity itself. Following Winton et al. (2013), we write:

$$v Q = v_0 Q_0 + v' Q_0 + v_0 Q' + v' Q' , \quad (1)$$

where Q_0 and v_0 are the steady state values of the quantity Q and the transport velocity v (including advection, diffusion and convection), and Q' and v' are their deviations. Here, Q can be any quantity transported in the ocean, e.g., temperature, salinity, 205 heat, etc. We consider the heat content density:

$$Q = C_p \cdot \rho_0 \cdot T, \quad (2)$$

where $C_p = 3981 \text{ J kg}^{-1} \text{ K}^{-1}$ is the specific heat capacity, $\rho_0 = 1027 \text{ kg m}^{-3}$ is the reference water density obtained from the average seawater density in steady state, and T is the potential temperature. With Q as heat content density, the first term on the right hand side of Eq. (1) represents the steady state heat transport, the second and third terms, $v' Q_0$ and $v_0 Q'$, quantify anomalous heat transport due to changes in circulation and in SST, respectively. The last term $v' Q'$ is quadratic in the deviations and hence small. Based on an analysis of global means in a climate change experiment with a 1 % per year increase in CO_2 and evaluated at year 100, Winton et al. (2013) give an estimate of $v' Q_0 : v_0 Q' : v' Q' = 1 : 0.3 : 0.1$. 210

We can find the contribution of each term in Eq. (1) by making use of experiments OcTRA ($v' \neq 0$) and OcFIX ($v' = 0$): $v_0 Q_0$ is calculated from OcTRA or OcFIX at year 1200; $v' Q$ from the difference between the two, i.e., OcTRA – OcFIX; 215 and $v_0 Q'$ results from the difference of OcFIX and its steady state, i.e., OcFIX – OcFIX($t = 1200$). The sum of all these indeed corresponds to OcTRA, which equals $v Q$. As mentioned by Winton et al. (2013), it is not possible to separate the terms $v' Q = v' Q_0 + v' Q'$, because the model only exhibits changing circulation v' under $Q' \neq 0$ as otherwise surface density is unchanged. A difference between this study and Winton et al. (2013) is that in our setup Q' is the same for fixed and for transient simulations, since it is determined by the prescribed SSTs, which are identical for OcFIX and OcTRA.

220 The decomposition of the northward global heat transport $v Q$ is shown in Fig. 5. The response of the meridional heat flux during the medieval cooling occurs primarily in the southern hemisphere and is caused by a strengthening of the circulation in the SO and Indo-Pacific and hence a stronger southward [heat](#) transport with only small changes in the Atlantic basin. The industrial warming is characterized by a decreasing poleward heat flux in both hemispheres. In the south, this is primarily due to changes in the Pacific circulation and changing SST and circulation in the SO. In the northern hemisphere, the weaken- 225 ing poleward heat transport is due to changes in the Atlantic Ocean. Here, changing circulation dominates in the form of a weakening overturning, which is only partly compensated by anthropogenic warming of the upper ocean.

We compare the meridional heat flux anomaly due to changing circulation during the industrial warming phase (Fig. 5b) to Winton et al. (2013), their Fig. 5 (bottom, black line). The shape of [the this](#) redistribution heat transport in our Fig. 5b is comparable to Winton et al. (2013), but it is about an order of magnitude smaller. [In the The](#) warming experiment of Winton 230 et al. (2013) [, the radiative forcing is is driven by a 1% CO₂ increase per year for 100 years, which corresponds to a radiative forcing of 4.5 Wm⁻²](#), whereas the radiative forcing in our experiment is only 1.4 Wm⁻². [The redistribution heat transport](#)

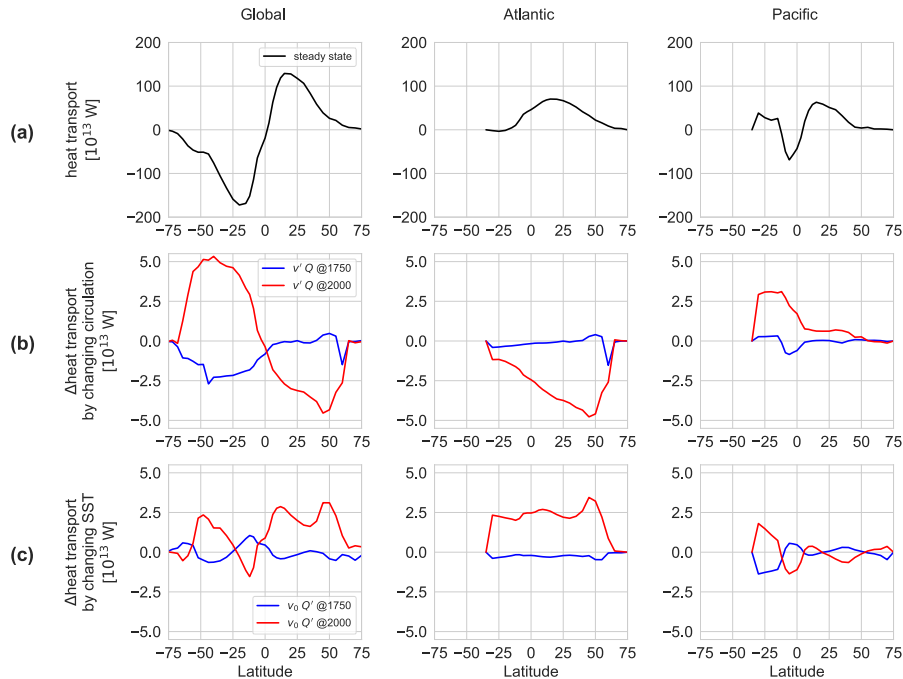


Figure 5. (a) Global and basin northward meridional heat transport in the ocean at steady state, OcFIX($t = 1200$). Meridional heat transport anomaly due to (b) changing circulation, and (c) changing SST. The coldest time of the LIA is shown in blue (1750 CE) and the industrial warming phase in red (2000 CE). Note the different order of magnitude on the y-axis. Results are derived from simulations OcTRA and OcFIX (see text) and variables v and Q refer to Eq. (1).

could also be smaller in our case because atmospheric processes are better represented in GCMs (general circulation models), such as the GFDL model used in Winton et al. (2013). The hydrological cycle of the Bern3D EMIC model reacts too weakly compared to another GCM, CESM version 1.0.1, for an ensemble member over the past millennium. Here the Bern3D SSS anomalies were an order of magnitude too low, although showing the same qualitative patterns.

In addition to heat transport, the column-integrated heat content density per unit area, hereafter called ocean heat areal density (OHD), informs about the distribution of heat uptake. OHD is given as

$$\text{OHD} = \int_{-H}^0 C_p \rho_0 T dz, \quad (3)$$

where H is the total height of the water column. OHD anomalies in year 1750 and 2000 are shown in Fig. 6. The medieval cooling causes a decrease in OHD globally (except in the Arctic in TRA), with relatively homogeneous cold anomalies in TRA, whereas FIX possesses the strongest cooling in the Atlantic in year 1750. For FIX, the 550 years of cooling were not enough to reach the old waters in the deep Pacific, but in TRA stronger Pacific anomalies are caused by circulation changes, which overlay the steady state transport of anomalous heat. In 2000 CE compared to 1205 CE (Fig. 6b, e), FIX still bears the

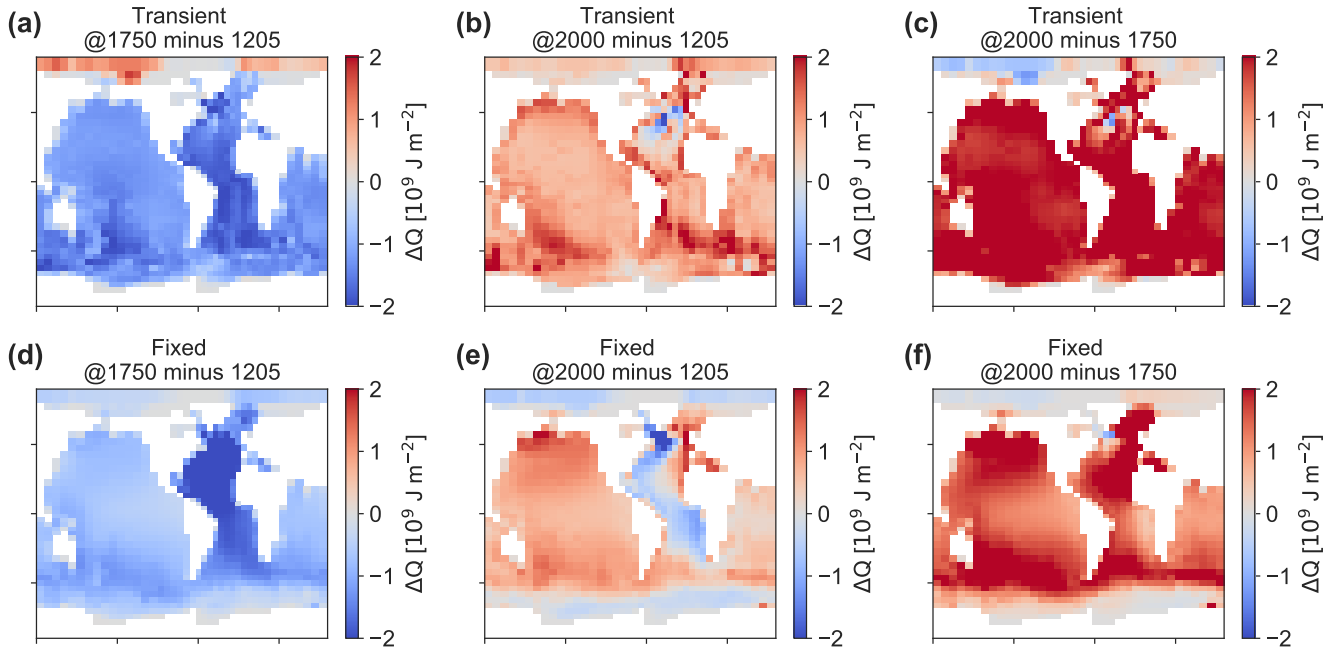


Figure 6. Ocean heat areal density (OHD) anomalies for transient and fixed circulation. (a), (b) Anomalies in 1750 and 2000 CE, both with respect to year 1205 for case OcTRA and (d), (e) for case OcFIX. (c), (f) Anomalies in 2000 CE are also shown with respect to year 1750.

signature of the LIA in the Atlantic, Arctic and SO. In TRA, this heat deficit has disappeared with the exception of a small region in the North Atlantic. It is evident that the transient response of the circulation determines the magnitude and regional distribution of the memory of past sea surface temperature anomalies.

Comparing OHD in 2000 CE to 1750 CE instead (Fig. 6c, f) and hence only considering anomalies during the warming period, gives a different picture. All heat anomalies are much larger, since the LIA cooling is not subtracted in this case. In TRA the OHD anomalies are larger than in FIX, confirming once more our finding that signals are propagating more effectively, i.e., with a larger amplitude, into the ocean in TRA than in FIX. Further, hardly any negative anomalies are present anymore in TRA and FIX in 2000 when taken with respect to 1750. That is, the warming hole in TRA (Fig. 6b) mainly originates as a residual from the 1200-1750 LIA cooling and is not due to the AMOC slowdown from 1750 to 2000 in our ocean-only setting.

The global ocean heat content (OHC) is given by $OHC = \int OHD \, dx \, dy$. The contributions of circulation and SST changes are determined by taking the difference between OcTRA and OcFIX respectively taking the anomalies of OcFIX with respect to its steady state. The result is given in Fig. 7. The decrease of OHC during the LIA is clearly dominated by changing SST, which globally has an effect about three times larger than changing circulation. During the warming, changing circulation and changing SST have a similar influence on a global scale with a slight dominance of the former before about 2300 CE; afterwards changing SST takes over to some extent, because the effect of changing circulation decreases with recovering AMOC. The time evolution of the partitioning of OHC into circulation and SST related anomalies is different in the two basins (Fig. 7b, c). The

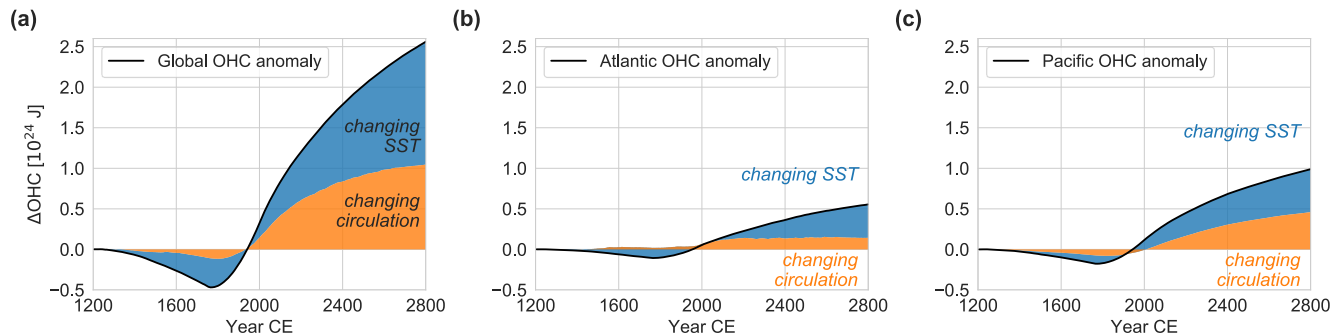


Figure 7. Ocean heat content anomaly decomposed in contributions due to changing SST and due to changing circulation for (a) the global ocean, (b) the Atlantic and (c) the Pacific basin, derived from simulations OcTRA and OcFIX.

260 medieval cooling of OHC is completely dominated by SST changes in the Atlantic, whereas the Pacific features an about equal contribution of circulation and SST related changes. The two effects contribute significantly in both basins under industrial warming, with a larger component of changing SST in case of the Atlantic. As expected, changing SST contributes in both basins to an OHC decrease under LIA cooling and an increase under global warming. In contrast, changing circulation has an unexpected effect in the case of the Atlantic under the LIA cooling: it slightly counteracts the global cooling. This is also
 265 visible in Fig. 6, where the Atlantic cooled more in OcFIX (panel d) than in OcTRA (panel a).

In the previous, we decomposed heat transport and OHC into the contributions of changing circulation and changing SST. Recall that the Hovmöller diagrams in Fig. 4a, b presented basin-averaged temperature anomalies over depth. These temperature anomalies, which are directly related to OHC (Eq. (3)), can readily be decomposed as well: the OcFIX anomalies in Fig. 4b already equal the contribution of changing SST, and the contribution of changing circulation is found by subtracting column
 270 OcFIX from OcTRA. The result (Fig. A2) confirms that changing SST causes the expected downward propagation of cooling respectively warming, whereas changing circulation causes the persistent cold anomaly in the Atlantic around 3 km depth with an enhanced warming above and below this depth in addition to an enhanced warming after 2000 CE in the Pacific and SO.

3.4 Explaining the leads and lags

Now we turn our attention to deep ocean temperature and the effects acting on it in a more local framework: our aim is to
 275 gain more understanding of the leads and lags that we observed at 3.1 km depth in the different basins in Fig. 4. ~~Instead of a true decomposition, we present a rough estimate of each contribution. Moreover, we split the effect of changing circulation. We distinguish three effects that influence deep ocean temperature: 1) the history of SSTs; and 2) changing circulation that we now split in two subeffects: 2a) shifts in water mass distribution, which determine whereto regional SST anomalies are carried, and 2b) the absolute overturning rate, i.e., how fast deep ocean water is replenished. The results are summarized in this Section, we discuss these effects qualitatively with the help of Figures 1b, 8 and 9. In Supplementary Sect. B, rough quantitative estimates of these effects are computed (results in Table B3 and explained below.; interpretation in Sect. B5).~~

280

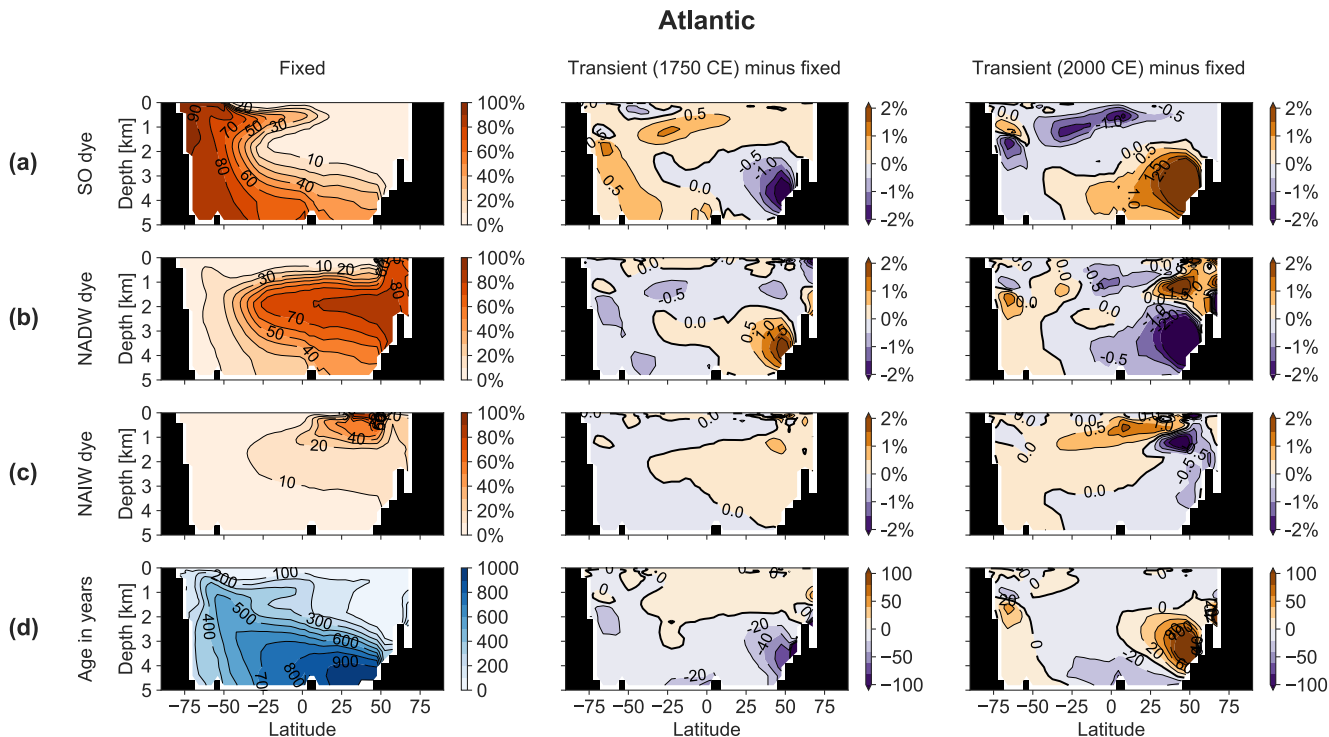


Figure 8. Zonally averaged meridional section of the Atlantic basin, including the SO sector, showing (a) Southern Ocean dye tracer, (b) North Atlantic Deep Water dye tracer, (c) North Atlantic Intermediate Water dye tracer and (d) ideal age. Columns show the fixed-circulation simulation (OcFIX) and the anomaly of transient (OcTRA) w.r.t. fixed in 1750 (coldest time in LIA) and 2000 CE. Units for dye are % of initial dye surface concentration.

Quantification of how different effects act on the deep ocean temperature at 3.1, per basin and at times of interest 1750 CE and 2000 CE. Values are temperature anomalies w.r.t. 1200 CE in centi-Kelvin (°C) and percentages are added in parentheses, where the residual is excluded, i.e., 100 % corresponds to the sum of effects 1, 2a, 2b and their interaction. For the percentage, the absolute value of each contribution is taken. Calculations and uncertainties are explained in Appendix B. **Multiple effects**

285 **1. Changing SST 2. Changing circulation^a Interaction^b Residual^c Total^d @3.1 km on:** 1. History of SST 2a. Water masses

2b. Water age Atlantic: 1750 -4.9 (57%) 3.5 (41%) -0.17 (2%) -0.004 (0%) 0.18 -1.32000 -3.3 (32%) -2.0 (19%) -5.0 (48%)
 -0.025 (0%) -3.7 -14.1 Pacific: 1750 0.011 (1%) -1.1 (97%) 0.023 (2%) -0.0001 (0%) -1.5 -2.62000 -0.46 (26%) -1.3 (72%)
 -0.038 (2%) -0.002 (0%) -2.2 -4.0 Southern Ocean: 1750 -0.97 (25%) -2.9 (74%) -0.059 (1%) -0.006 (0%) -2.5 -6.52000
 290 -6.1 (73%) 2.2 (26%) 0.008 (0%) -0.006 (0%) 4.6 0.72

Firstly, historical SST anomalies differ between regions such that deep water formation regions experience different surface temperature trends. As an illustration, we refer back to Fig. 1b for our idealized forcing. Recall that regions are defined in Fig. A1 and correspond to the source regions of different dye tracers. We notice relatively high amplitudes in the North Pacific and

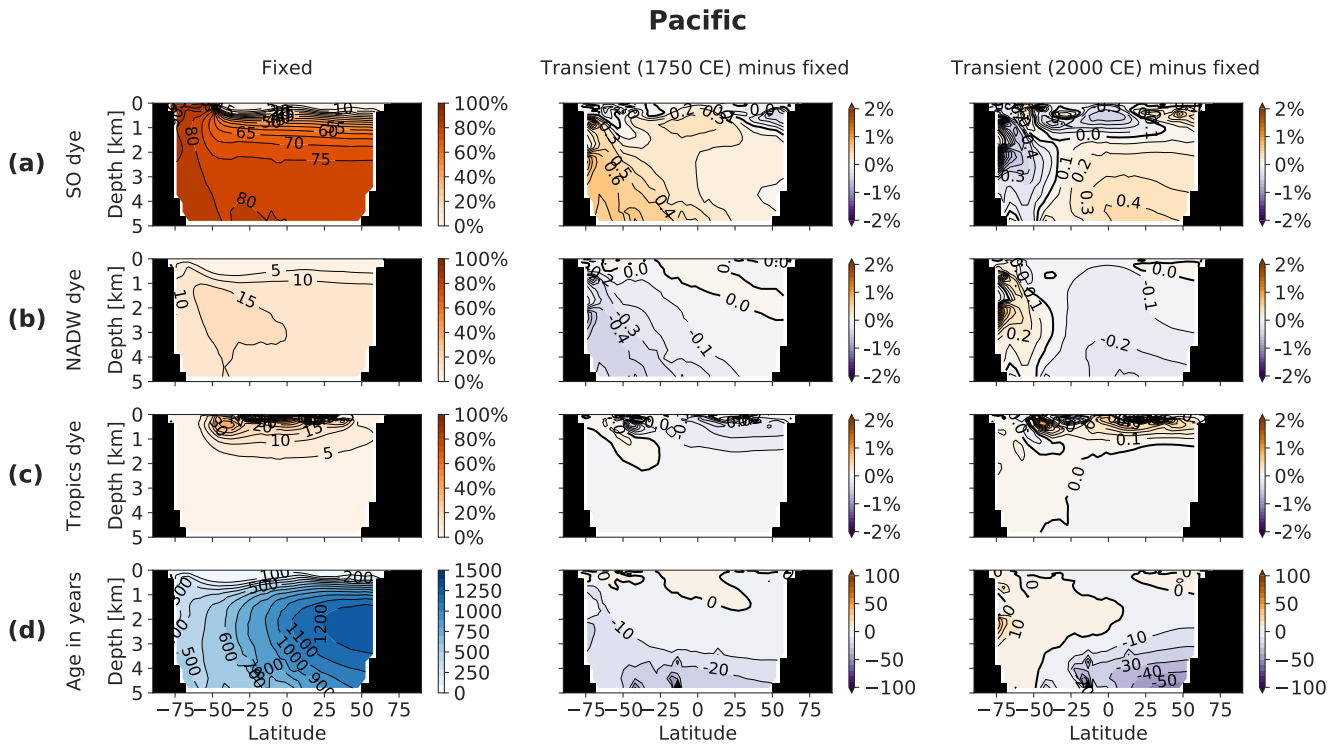


Figure 9. Zonally averaged meridional section of the Pacific basin, including the SO sector, showing (a) Southern Ocean dye tracer, (b) North Atlantic Deep Water dye tracer, (c) tropics dye tracer and (d) ideal age. Columns show the fixed-circulation simulation (OcFIX) and the anomaly of transient (OcTRA) w.r.t. fixed in 1750 (coldest time in LIA) and 2000 CE. Units for dye are % of initial dye surface concentration. Colour levels for Pacific anomalies increase in steps of 0.1 % dye or 10 years age, respectively.

South Atlantic, and low amplitudes in the Arctic, but these regions play a minor role in determining the ocean temperature at
 295 depth. The larger variability of northern North Atlantic SST is due to convection occurring in only 40 grid cells there. This
 region's SST (NADW formation) sees no clear cooling during the first two centuries, but catches up with the global average
 cooling trend afterwards. The Southern Ocean SST (AABW and AAIW) starts cooling rapidly, but with a smaller amplitude
 than the global average. Comparing these two most important water masses, we conclude that NADW sees less of the LIA
 cooling than AABW during 1200-1400 CE, but more during 1500-1750 CE. ~~The effect of SST history (effect 1) at a fixed 3-1
 300 depth is computed (Table B3), where the SST history of all 8 water masses is taken into account (Appendix B). Evidently,
 effect 1 contributes a cooling in 1750 CE in the deep Atlantic and SO, but no SST-caused cooling reaches the deep Pacific yet.
 In 2000 CE, the cooling contribution reached the deep Pacific and is still present at this depth in all basins.~~

Let us turn to effect 2a, shifts in the distribution of water masses, which are illustrated by means of dye tracers. The merid-
 305 ional distribution of the water masses that dominate the abyss is shown in Fig. 8a-c (Atlantic) and Fig. 9a-c (Pacific). We track
 the combined water masses of AABW and Antarctic Intermediate Water (AAIW) with one Southern Ocean dye (SO). First

we discuss the changes in 1750: the largest water mass changes occur in the North Atlantic at 3 km depth, where the NADW fraction increases by about 2 percent points at the expense of AABW (3°C colder than NADW). This has a warming effect that counteracts the LIA cooling in the Atlantic. In the deep Pacific however, slightly more AABW flows in from the south at the expense of NADW. Analogously, this has a cooling effect and enlarges the propagation of the LIA cooling in the transient case. ~~Table B3 confirms that effect 2a, shifting water masses, leads to a warming in the Atlantic and a cooling in the Pacific at 3.1. Note that here all water masses are taken into account such that a second-order effect is present: relatively more deep water formation water masses (NADW and AABW) relative to other water masses under the LIA forcing, which leads to an additional cooling.~~ In the year 2000, ~~we see a cooling in the Atlantic and Pacific at this depth, whereas the SO warms. Dye dye tracers in the Atlantic reveal a pattern that is opposite to 1750, so they track a cooling at 3.1 km depth. Water mass anomalies in 2000 south of 35 show that the SO warming is caused by more NADW-sourced water and less local SO water. It is surprising that in the~~ In the Pacific (excluding the SO sector), the same qualitative water mass anomalies as in 1750 are still present, however displaced northwards, ~~and opposite.~~ ~~This slower water mass renewal is due to the longer residence time of waters in the Pacific. Opposite~~ trends are developing in the SO. This is because of a delay: the amount of SO water mass is already decreasing in 2000 (and NADW increasing) but the decrease initiated only around 1900 CE, such that the water mass anomaly built up over 1200-1900 CE is not compensated for yet (not shown).

Effect 2b is the absolute overturning rate, estimated by changing water age. In principle it is possible that the rate at which water masses refresh would change without any change in the relative composition of water masses. For instance, AABW and NADW would then still be present in the same proportion, but a general speed-up of the circulation (a faster overturning) would make the water age younger. Intuitively, a strengthening of the global MOC brings more cold polar surface water to the abyss resulting in a global cooling of the deep ocean, because downward heat diffusion from low-latitude surfaces is opposed by upwelling of colder deep water. From the ideal water age in 1750 CE in Fig. 8d and Fig. 9d, we see that the water becomes younger by up to ~ 40 years in the deep Atlantic and up to ~ 10 years in the deep Pacific at 3 km depth. In 2000 CE, the age anomalies are in the other direction, as expected: the deep North Atlantic ages by more than 100 years, whereas the Pacific SO becomes ~ 5 years older. The rest of the Pacific continues to become younger, which is again due to a delay and the water will become older, with respect to 1200 CE, in 2100 CE (not shown). We conclude that effect 2b causes the deep Atlantic to see an older, hence warmer, signal during the LIA cooling and a younger, hence colder (noting that the ~ 500 yr old water in 2000 CE still sees SSTs of 1500 CE), signal during the warming period after 1750. This contributes to a delay during both periods. We expect that the influence in the Pacific and SO is minor because of the small changes in age. ~~For effect 2b, many values in Table B3 have different signs than expected based on the above analysis of ideal age changes. We conclude that the values indicated as $\leq 2\%$ are indeed not significantly different from zero. Thus, This is confirmed by Sect. B5, which states that effect 2b has a very small impact at 3.1, except in the only has an impact that is significantly non-zero in case of the Atlantic in 2000, where we also observed the largest change in ideal age.~~

~~Finally, we assess the relative contributions of effects 1, 2a and CE, in which case it indeed leads to a strong cooling. This effect 2b at 3.1 (Table B3). Surprisingly, the change in absolute overturning rate, which is estimated via water age, has~~

340 ~~practically no influence in all cases except the Atlantic is even the main cause of the persistent cold anomaly in the deep Atlantic (Fig. A2a): estimated as 48% in addition to 32% of the cooling by effect 1 and 19% by effect 2a).~~

~~Summarizing the above and Supplement B, we can explain the strong lag, i.e. persistent cold anomaly, in 2000 CE. In all other cases, deep ocean temperature anomalies are determined by the interplay of SST and water mass changes. In the Atlantic, the deep Atlantic (Fig. 4d). Here SST and water mass changes counteract each other in 1750: they contribute roughly equally~~
345 ~~in 1750 but with opposite signs. Therefore, the shifted water masses cause a, causing this significant~~ delay in the arrival of LIA cooling at depth until 1750. ~~In the LIA cooling. In the year 2000, both water masses and water ages now strongly enhance the effect of water ages comes into play and together with changing water masses now strongly enhances~~ the amplitude of the cooling, which arrives relatively late. ~~As such, the arrival of the industrial warming is delayed as well. These mechanisms explain the two-century lag observed in the Atlantic and nicely correspond to Fig. 4d, where we see the amplitude of TRA dampened until 1750 but enhanced until 2000 (and further).~~
350 ~~In the Pacific and SO, the contribution of water mass changes generally dominates over SST (except for the SO in 2000). These no counteracting effects are observed. SST and water mass changes contribute with the same sign as the forcing such that they fasten and enhance both contribute a cooling such that~~ the arrival of anomalies at depth. ~~This explains the leads observed in the Pacific and SO and the larger amplitudes in the LIA at depth is fastened and enhanced, which explains the observed leads and the larger amplitude for TRA.~~

355 4 Sensitivity of leads and lags

The leads and lags of temperature minima from the LIA cooling (Fig. 4c, d) are determined by model-dependent changes in circulation, including advection, diffusion and convection. In this Section, we test how robust the leads and lags are under varying key model parameters for mixing and wind. We run additional transient and fixed simulations with halved and doubled mixing, respectively wind stress (Table 1). The changes are applied globally and uniformly. Figure 10 summarizes the resulting
360 leads (negative) and lags (positive) throughout the water column of TRA with respect to FIX simulations.

An overall picture appears of leads in the Atlantic that are interrupted by a depth range of lags, and leads throughout the Pacific and SO. These lags in the Atlantic are located between about 2.5 and 4 km for standard, weak mixing and strong mixing simulations, but they are shifted upwards for weak and strong wind, from 1.5 to 3 km and from 1.5 to 2 km, respectively. Therefore, our finding that changing circulation delays the propagation of the downward signal in a certain depth range in the
365 Atlantic but accelerates it everywhere else is robust, with the precise depth range boundaries depending on model parameters.

At a fixed 3.1 km depth, the leads and lags are relatively robust under varying mixing, but not under varying wind, especially in the Atlantic. The diapycnal diffusivity K_d is halved or doubled to vary mixing (Fig. 10b, c). In the Atlantic, weak mixing has not much influence, but strong mixing makes the ~ 226 yr lag almost disappear. This is explained by the presence of two local temperature minima in the Atlantic for OcFIX (Fig. 4b), OcFIX_weakmix and OcFIX_strongmix. Only in the case of
370 OcFIX_strongmix, the global minimum, which is marked to compute the lag, is shifted towards the second local minimum. A change in FIX compared to the standard simulation OcFIX is possible at all, since the steady states for weak and strong mixing are different (Fig. A4-A5). Lead times in the Pacific and SO stay within the range of 125 to 150 years and are hence insensitive

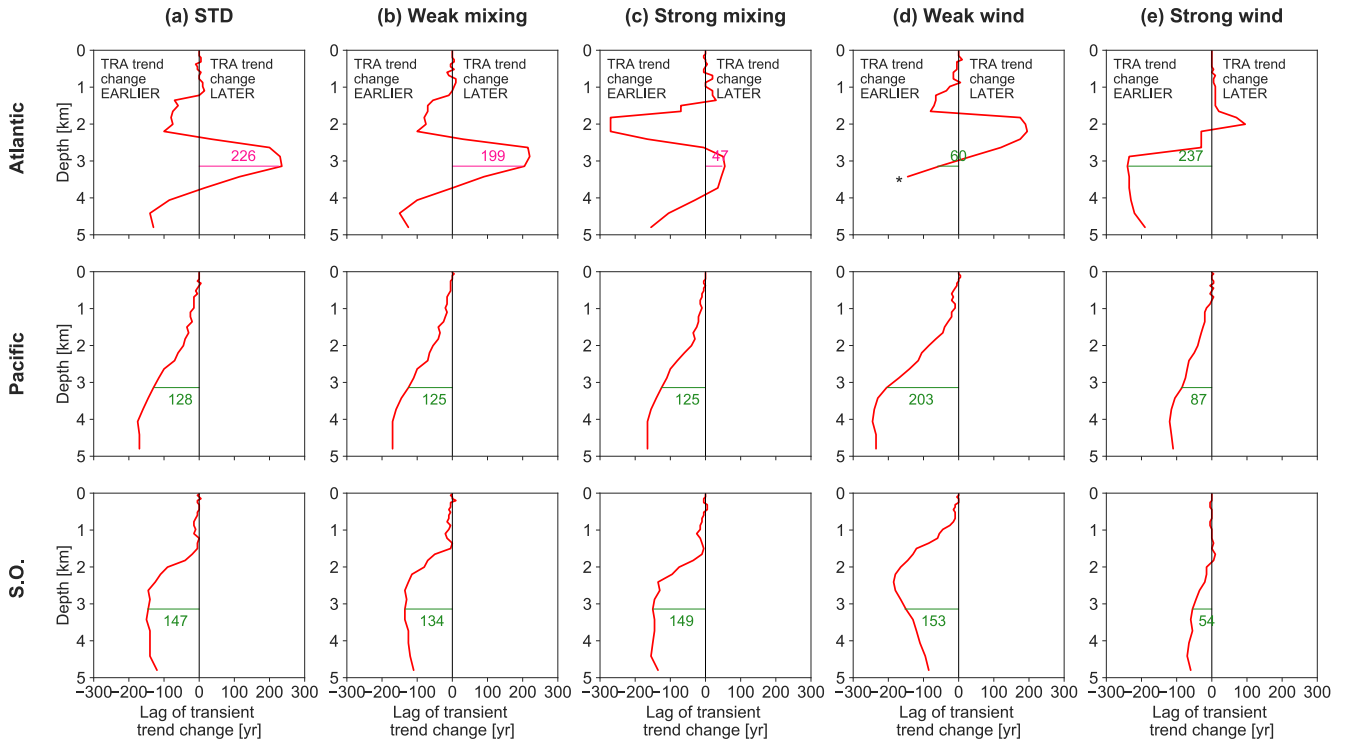


Figure 10. Lags (positive) or leads (negative) in the arrival of the warming at each depth (transient minus fixed simulation). Results are shown for (a) the standard simulations OcTRA and OcFIX (repeated from Fig. 4c), (b, c) simulations with varying mixing (OcTRA_weakmix and OcFIX_weakmix respectively OcTRA_strongmix and OcFIX_strongmix) and (d, e) varying wind stress (OcTRA_weakwind and OcFIX_weakwind respectively OcTRA_strongwind and OcFIX_strongwind). Numbers indicate the values of leads and lags at 3.1 km depth. *For (d), the red line stops in the Atlantic below 3.4 km, because the LIA cooling anomaly is not detectable in OcFIX_weakwind at these depths such that its trend change is undefined.

to these rather large changes in K_d . Steady states possess especially different MOCs for halved and doubled wind stress τ_{wind} . Increasing wind stress almost doubles the MOC in the northern hemisphere and creates a strong Deacon cell in the SO, i.e., Ekman-driven equatorward flow. This causes large differences in simulated leads and lags for varying wind (Fig. 10d, e). The lag in the Atlantic becomes a lead instead, whereas the leads in Pacific and SO range from about 50 to 200 years.

For the standard simulation, amplitudes of LIA cooling were considerably larger in TRA than in FIX at 3.1 km depth, as noted previously in Fig. 4d. This property is robust under varying mixing and wind: all sensitivity simulations possess larger TRA than FIX amplitudes at 3.1 km in all basins, except strong wind in the Atlantic (not shown). Thus, circulation changes enhance the amplitude, hence detectability, of deep ocean temperature anomalies.

5 Comparison to Gebbie and Huybers (2019)

Our study was motivated by the earlier study of Gebbie and Huybers (2019) (GH19, henceforth), who interpreted deep ocean temperature anomalies with an inverse model with fixed circulation, inferred from oceanographic measurements from the late 19th century and modern observations. Early transects in the Atlantic and Pacific oceans are available from the expedition of the HMS *Challenger* of 1872-1876, and modern data were obtained during WOCE in the 1990s. As a result, the circulation state in the model of GH19 corresponds well with observations and with measured ventilation rates. GH19 have identified coolings and warmings at a depth range of 1800 to 2600 meters, which they attribute to remnant deep ocean signals of surface climate change. They find that the deep Pacific has been cooling during that period, but the deep Atlantic, particularly in the northern hemisphere, has been strongly warming.

We refer back to the basin-averaged Hovmöller diagrams in Fig. 4a-b, a, b. These compare directly to Fig. 4b-e-1c, b from GH19, though with a different time axis: we show 1200 – 2800 CE, whereas they simulate 0 – 2000 CE, including a medieval warm period around 600 CE. The downward propagation of temperature anomalies in the Pacific qualitatively agrees between the two studies. The result of GH19 in the Atlantic is qualitatively similar to our FIX case but not to TRA, which is as expected since their model has a fixed circulation. This confirms again that the persistent cold anomaly in the deep Atlantic observed for the Bern3D TRA originates from circulation changes, i.e., from an increase in southern sourced water at this depth (Fig. A3). We expect that most models with transient circulation show this behavior under AMOC slowdown, but the strength and timing of the persistent cold anomaly will be model-dependent. Quantitative amplitudes of deep ocean cooling until 2000 CE are similar in the Pacific in the two studies, but GH19 show slightly stronger cooling in the Atlantic (up to 20 cK instead of 15 cK), which also extends deeper.

Now we answer the question whether in the simulations the deep ocean (2 km and deeper) at present is still cooling from the LIA or already warming. Recall that the red lines in Fig. 4a-b, a, b help us identify whether the deep ocean at present (2000) is still cooling (red line to the right of 2000) or already warming (red line to the left of 2000). GH19 predicted that the deep Pacific is still cooling at present, but the deep Atlantic already warming. For the Pacific, this is consistent with our FIX case but not with TRA, which is thought to be more realistic than FIX. In our study, most of the deep Atlantic water column is still cooling at present for both TRA and FIX (although the 2 – 3 km part is already warming in FIX). ~~This substantial difference between our study and GH19 in the Atlantic occurs because the deep North Atlantic is too old in the Bern3D ocean model compared to radiocarbon observations (Gebbie and Huybers, 2012), which correspond to the ages in the observation-based model of GH19. These observations show radiocarbon ages of up to 600 years in the North Atlantic (zonal average), whereas we find ideal ages over 900 years (Fig. 8). Therefore, our model needs more time to detect the warming in the deep Atlantic.~~

In addition, we reproduce Fig. 2 from GH19 (repeated in Fig. 11c) for the two cases of OcTRA and OcFIX, (Fig. 11a, b), which focuses on a depth of about 2 km (Fig. 11). Note that in our TRA case it makes a significant difference which depth we consider, whereas their anomalies travel down more uniformly over depth. At 2 km depth, the fingerprint of circulation changes is not as strong as for instance at 3 km. ~~Figure 11 shows~~ Figures 11a and b show a wide-spread warming trend from 1875 to 1995 CE in both cases in the North Atlantic. However, both cases also exhibit cooling a cooling trend during this time

415 interval in some limited areas of the North Atlantic. For TRA, cooling is simulated in the northeast Atlantic, whereas FIX shows cooling in the northwestern part of the North Atlantic. In the Pacific, warming (TRA) or cooling (FIX) trends are very small. In our FIX simulation, ~~cooling is still a cooling trend is~~ found in the Pacific, but it is rather weak, and the southwestern Pacific is ~~already warming warmer in 1995 compared to 1875 CE~~. The difference between *Challenger* and WOCE data, as well as the model simulation of GH19, ~~show (Fig. 11c), show a~~ clear remnant cooling trend in the Pacific in this depth range around
420 2 km.

The fact that the deep Pacific cooling is weak in our simulations could be caused by the choice of our forcing, which is simpler than that used by GH19 with less climate fluctuations and has a slightly smaller industrial warming amplitude. We have ignored climate variations before year 1200 ~~and start with the medieval cooling from 1200 to 1750. Their simulation starts, whereas GH19 start~~ at 0 CE and ~~has an approximate global mean warming of 0.2 over 600 years with a subsequent~~
425 ~~cooling. Signals from this simulate an~~ early medieval warm period ~~also propagate into the deep Pacific, and we hypothesize that this would be able to delay the arrival of the later cold LIA anomaly in this region, producing that notable difference before~~
1200. An additional Bern3D experiment (simulations OcTRALong, OcFIXLong) with a medieval warm period before 1200 (similar in amplitude to GH19) showed that this does not alter our main results. Figures A6a and b only show subtle differences compared to Fig. 4a, b from ca. 1600 CE onward. For example, the preceding medieval warm period delays the arrival times
430 of the temperature minimum in the Atlantic between 2 and 3 km by only 10 (FIX) to 35 (TRA) years. A notable difference is also that the cooling in the Pacific no longer penetrates below 2 km for OcFIXLong (in the case of OcFIX the cooling here was less than 5 cK).

6 Conclusions and outlook

Understanding the evolution of deep ocean temperature brings insight into the ocean heat content and its rate of change, and
435 is important for the initialization of historical and present-day simulations. We found that even the relatively small changes in ocean circulation during the last 800 years have a profound impact on deep ocean temperature. While changing ocean circulation fastens the arrival of cold and warm atmospheric temperature anomalies in the deep Pacific and deep Southern Ocean (SO), it delays the arrival of this signal in the deep Atlantic between about 2.5 – 3.5 km depth. This lag in the deep Atlantic is two centuries in our simulations and is caused first by a relative increase of NADW at the cost of AABW during
440 the LIA cooling, followed by an older water age under AMOC slowdown during industrial warming. Moreover, circulation changes enhance the amplitude of deep ocean temperature fluctuations in all three major basins, thus making atmospheric anomalies better detectable in the deep ocean.

We have decomposed heat transport and ocean heat content (OHC) anomalies into the contributions of changing circulation and changing SST. Poleward heat transport decreased under early industrial warming, in which the effect of changing circula-
445 tion was dominating. Our second decomposition showed that OHC anomalies were for about one third caused by changing circulation during the LIA cooling (hence two thirds by changing SST), whereas both effects had an approximately equal con-

tribution under industrial warming. We conclude that ocean heat uptake is not solely dominated by atmospheric temperature anomalies, but changing ocean circulation has a significant impact.

450 Lastly, we assessed the robustness of leads and lags under varying mixing and wind strengths. The transient simulation, where ocean circulation adjusts dynamically, still had a larger amplitude than the fixed-circulation simulation in almost all cases and basins. At the fixed depth of interest of 3.1 km, the circulation-caused leads in the deep Pacific and SO versus lags in the deep Atlantic were quantitatively quite robust under varying mixing, but not under varying wind stress. Throughout the water column, the qualitative result of leads in the Pacific and SO is robust under our sensitivity tests. The same holds for the interesting observation of leads in the Atlantic that are interrupted by lags at a certain depth range (either around 2 or around 3
455 km).

We are aware that our results are to a certain extent model-dependent ~~,-especially on the- and therefore we welcome more research concerning the propagation of past surface temperature anomalies to the abyss in other models.~~ The modeled age of deep waters and ~~on the~~ relative response of AMOC versus SOMOC strength under changing SST ~~.-Therefore, we welcome more research concerning the propagation of past surface temperature anomalies to~~ are especially important possible biases for this
460 study. In the Bern3D model, the abyss in other models. A deep North Atlantic is too old compared to radiocarbon observations (Gebbie and Huybers, 2012), which correspond to the ages in the observation-based model of GH19. These observations show radiocarbon ages of up to 600 years in the North Atlantic (zonal average), whereas we find ideal ages over 900 years (Fig. 8). The sensitivity simulations with strong mixing have a smaller bias in North Atlantic water age (maximum age ca. 800 yr) and still show a temperature propagation very comparable to Fig. 4 (not shown). We conclude that this model bias is likely
465 not responsible for the main differences between GH19 and our study. Another weakness of the coupled Bern3D model is the representation of atmospheric processes, in particular the hydrological cycle. As such, the generated time-varying SSS field could be replaced in future work by a more realistic SSS from another coupled model or via paleoreconstructions (e.g., the PHYDA database of Steiger et al. (2018)).

In this paper, we held ocean-atmosphere feedbacks ~~and total ocean heat uptake~~ identical between transient and fixed sim-
470 ulations, by prescribing the same SST and SSS time series. We needed this for a correct comparison of the propagation of (identical) sea surface temperature to depth. In reality, ocean-atmosphere feedbacks and SST patterns are different when the ocean circulation is allowed to dynamically adjust, i.e., in transient simulations (Winton et al., 2013). These effects come on top of the contribution of changing circulation we found. It would be interesting to find a way to combine our approach with the approach of Winton et al. (2013) such that deep ocean temperatures can be compared unbiased without losing the ability of
475 ~~including studying~~ different ocean-atmosphere feedbacks ~~and studying total OHC change.~~

In our case study of the past 800 years, we chose an idealized forcing, whereas Gebbie and Huybers (2019) used a forcing with more high-frequency SST fluctuations, which is more realistic but also harder to interpret. Moreover, one could use an even more realistic forcing by prescribing time-varying SST fields with trends that differ between regions, for example with different times of occurrence of the LIA, by obtaining them directly from recent paleoreconstructions (Neukom et al., 2019)
480 instead of from simulation OcAtmTRA. In a more general view, we would be able to understand how any historical SST record travels down to the deep ocean when we understand the effective depth to which surface temperature anomalies travel (Xie and

Vallis, 2011) as a function of the anomaly's frequency and amplitude, and depending on changes in ocean circulation that are a response to this cooling or warming.

485 *Code and data availability.* The Bern3D model is closed-source, but the output of all model simulations used in this study is available in netCDF format (Scheen et al., 2020). The analysis code that was used to make the figures and to perform the calculations in Appendix B is available as a well-documented python notebook (Scheen, 2020). In the case of questions or suspected bugs, please contact J.S.. For Fig. 11c, data were used from <https://www2.whoi.edu/staff/ggebbie/> > Downloads > Gebbie & Huybers (2019) data in figures > Figure2_GH19.nc, accessed 8 September 2020.

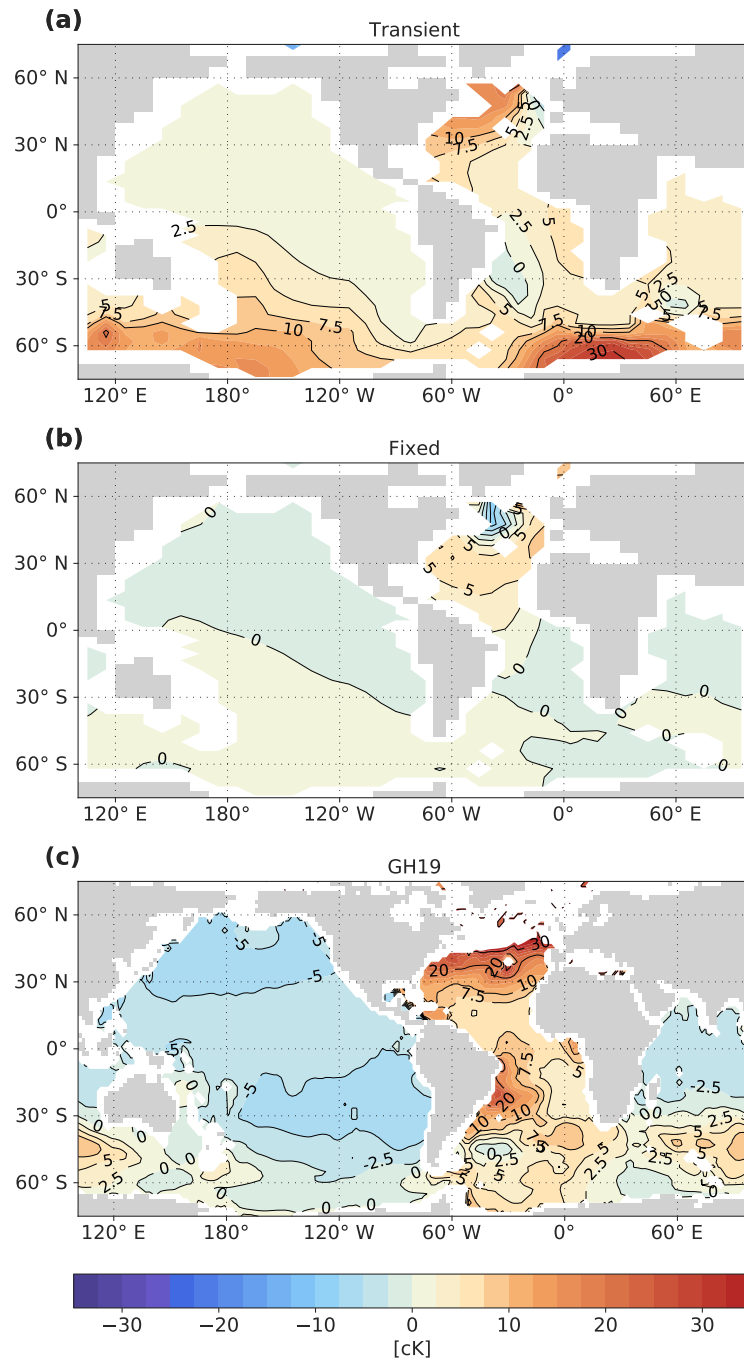


Figure 11. ~~Reproduction of~~ [Comparison with](#) Fig. 2 of Gebbie and Huybers (2019) for the two cases of transient and fixed circulation. Deep ocean temperature anomalies are determined between year ~~1875-1872-1876~~ (Challenger expedition) and ~~1995-1990-2002~~ (WOCE campaign) and averaged over the depth of ~~1912-1800 to 2520-2600~~ m, for ~~simulations~~ (a) [simulation](#) OcTRA (transient) and, (b) [simulation](#) OcFIX (fixed). ~~For comparison and~~ (c) [the model output of Gebbie and Huybers \(2019\), see Fig. 2 of Gebbie and Huybers \(2019\), repeated here for easy comparison.](#)

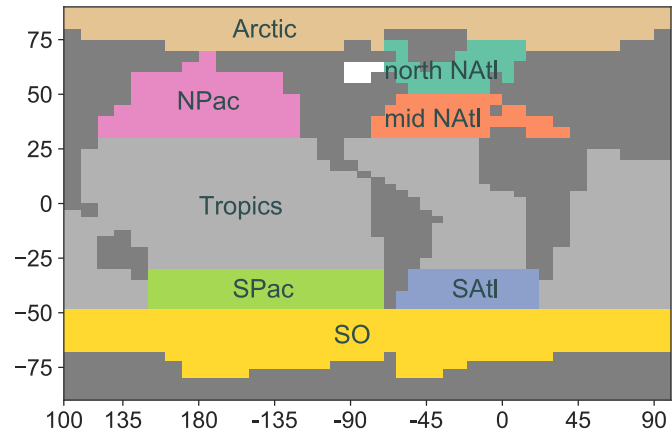


Figure A1. Definition of areas as used for regional SST averages on the Bern3D model grid (Fig. 1b, same colors). Simultaneously, these surface areas define where the 8 dye tracers originate (Fig. 8, 9 and A3). The dye tracers are named after the water masses they follow: Arctic, North Pacific Intermediate Water (NPIW, in the area NPac), Tropics, South Pacific Intermediate Water (SPIW, in the area SPac), Southern Ocean (SO), North Atlantic Deep Water (NADW, in the area north NATl), North Atlantic Intermediate Water (NAIW, in the area mid NATl) and South Atlantic Intermediate Water (SAIW, in the area SATl). Together they cover the whole ocean surface except the Hudson Bay. The SO dye tracer contains both AABW and AAIW.

A2 Figures regarding standard simulations OcTRA and OcFIX

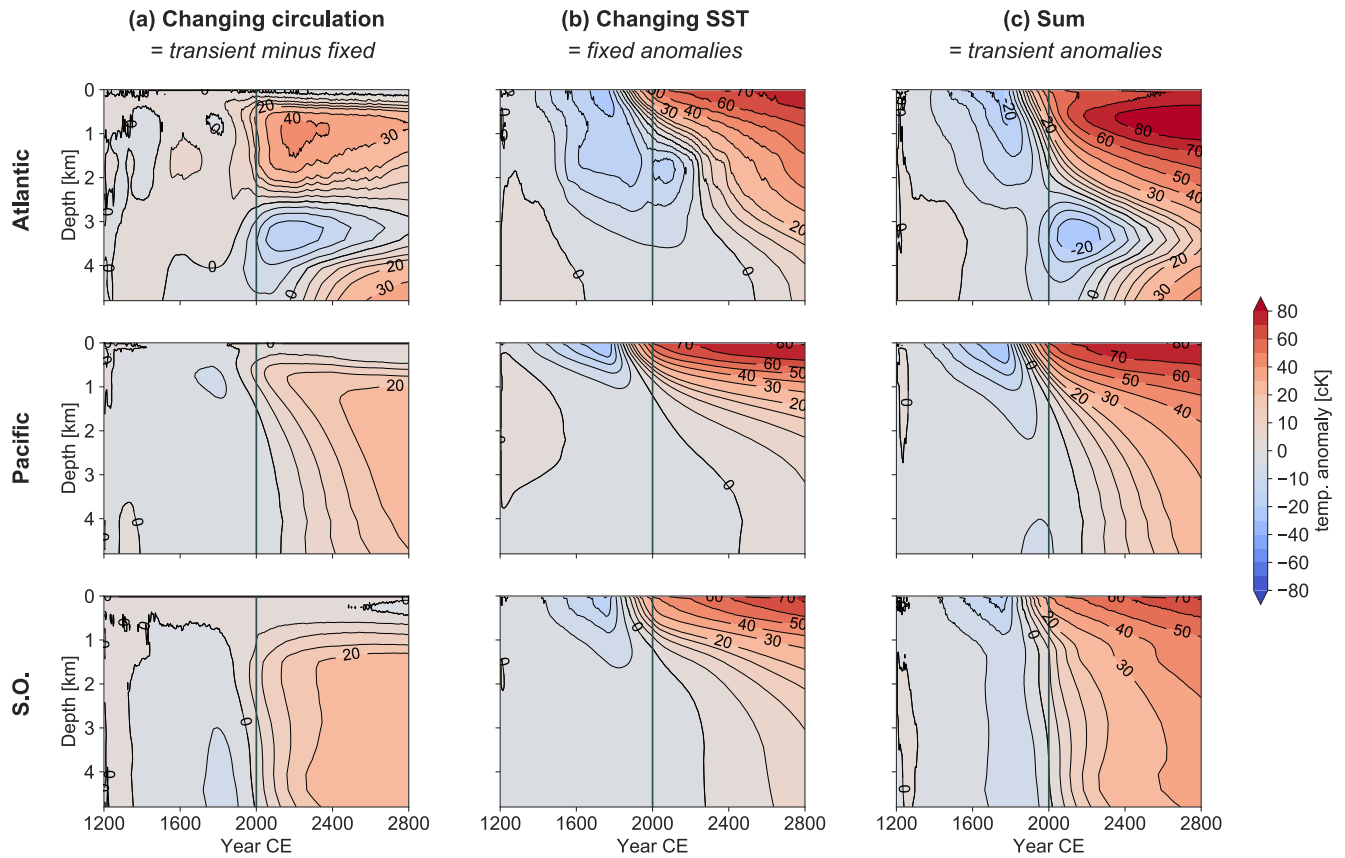


Figure A2. Hovmöller diagrams of temperature anomalies over depth, decomposed into the effects of **(a)** changing circulation and **(b)** changing SST with **(c)** the total. Columns (a), (b), (c) equal Fig. 4a minus 4b, Fig. 4b and Fig. 4a, respectively (see main text). Values are in centi-Kelvin ($1 \text{ cK} = 10^{-2} \text{ K}$) and are basin averages of the Atlantic or Pacific (35°S – 70°N) or the Southern Ocean ($< 35^{\circ}\text{S}$), respectively. Colour levels increase in steps of 5 cK from -20 cK to 20 cK and in steps of 10 cK otherwise.

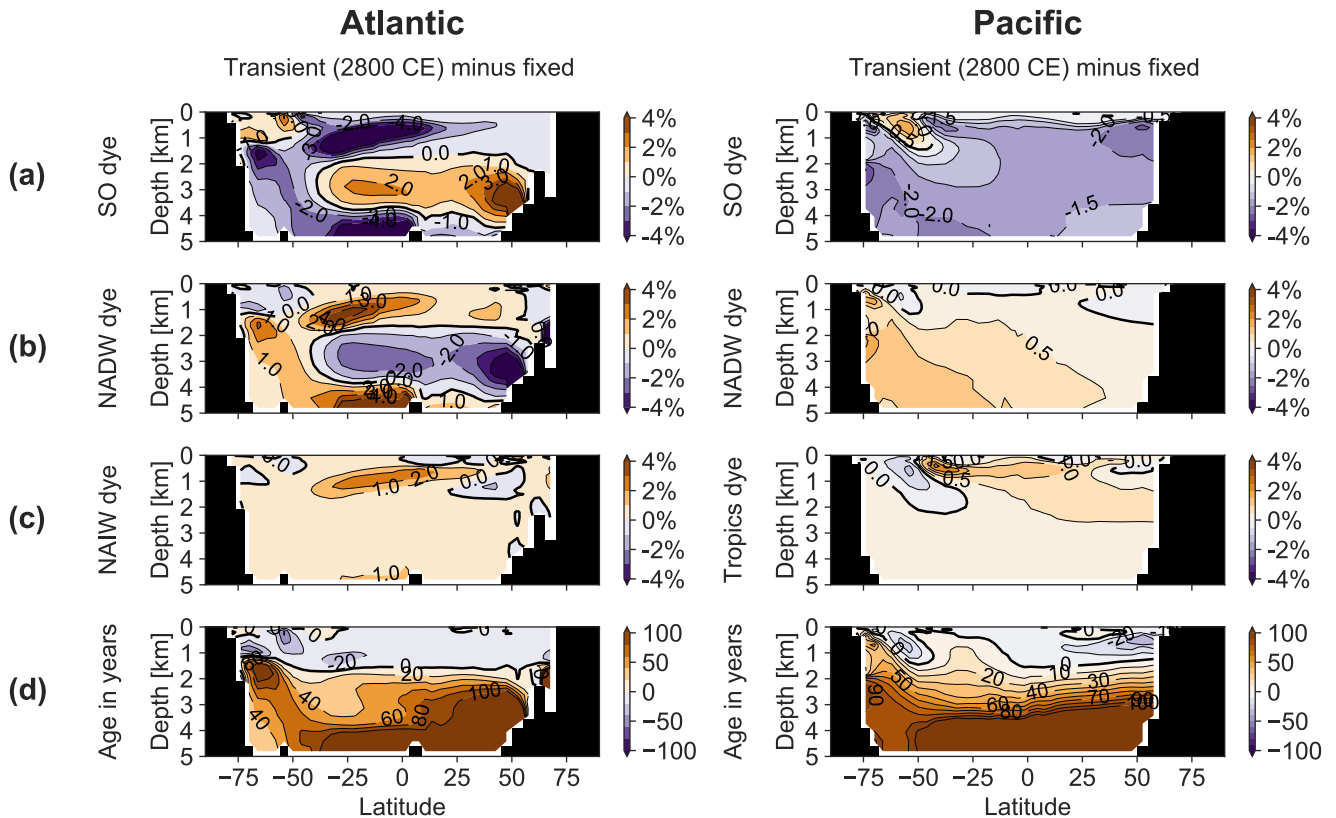


Figure A3. Zonally average meridional sections of the Atlantic respectively Pacific basin, including their Southern Ocean sector. Shown are the anomalies of transient (OcTRA) w.r.t. fixed (OcFIX) at 2800 CE (the end of the simulation) of (a) Southern Ocean dye tracer, (b) North Atlantic Deep Water dye tracer, (c) North Atlantic Intermediate Water dye tracer (for Atlantic) respectively Tropics dye tracer (for Pacific) and (d) ideal age. Units for dye are % of initial dye surface concentration.

This Fig. A3 shows that the water mass shift between SO dye and relatively warmer NADW in panel (a) and (b) explains the observed temperature propagation in the Atlantic (Fig. 4a), which shows a persistent cold anomaly between 2 and 4 km combined with enhanced warming above 2 and below 4 km depth. In this argumentation we used the fact that NADW dye tracer also reaches below 4 km, e.g., occupying 10-30 % of the water mass in the South Atlantic at this depth (Fig. 8b). This percentage is larger than expected, because NADW water travelling via the SO back into the deep Atlantic without touching the surface still retains the NADW signature.

A3 Figures regarding sensitivity-test simulations

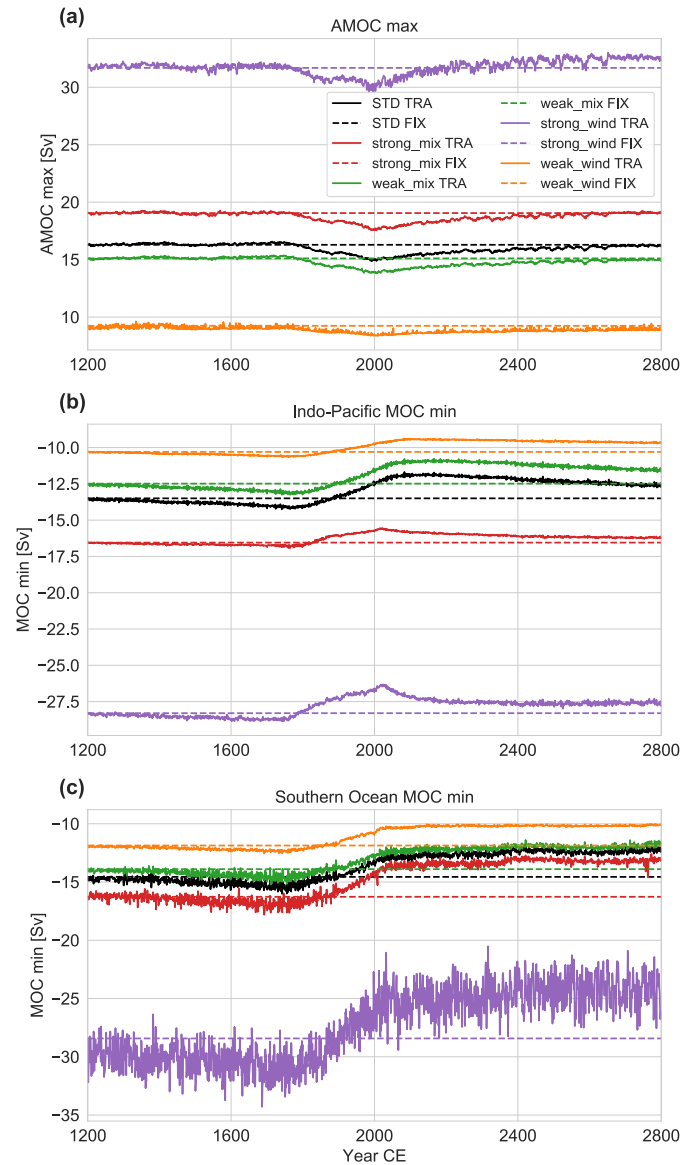


Figure A4. For simulations with varying parameters: (a) Atlantic Meridional Overturning Circulation (AMOC) maximum, (b) minimum of the MOC in the combined Pacific and Indian basin (IPMOC) and (c) in the Southern Ocean (SOMOC). Either the wind stress or mixing (i.e., diapycnal diffusivity parameter) is doubled, respectively halved. TRA stands for transient simulations and FIX for fixed-circulation simulations.

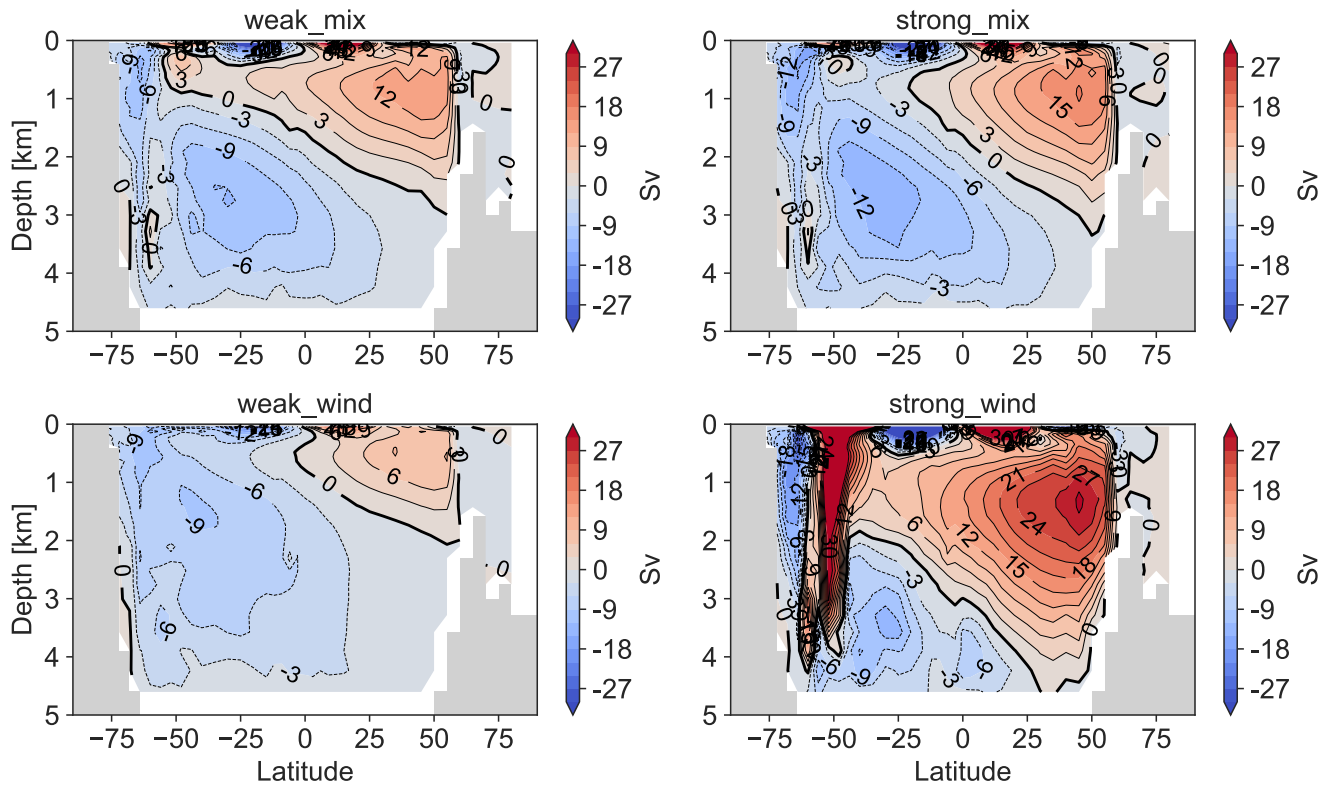


Figure A5. Global overturning circulation in steady state (15-year average) for sensitivity simulations (see Fig. 3c for the standard simulations). The overturning stream function is positive (red) for water rotating clockwise and negative (blue) for counterclockwise.

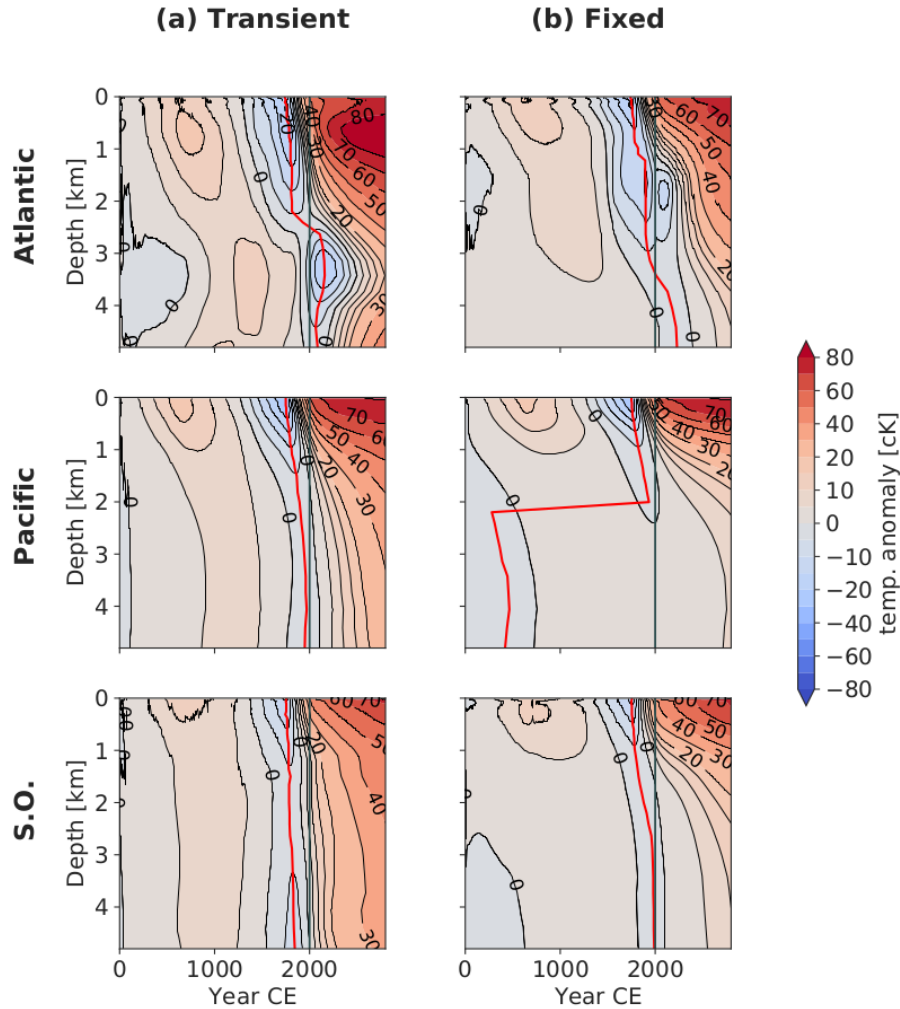


Figure A6. Hovmöller diagrams as in Fig. 4a, b (see caption there) but now for simulations (a) OcTRALong (transient) and (b) OcFIXLong (fixed). The minimum temperature anomaly (red line) jumps for fixed, because no cooling is detected in the Pacific below 2 km. Note the extended time axis from 0–2800 CE, because a medieval warm period (MWP) is now included.

For OcTRALong and OcFIXLong, SST/SSS/sea ice boundary conditions are read in from a coupled simulation OcAtmTRALong starting at 0 CE with a MWP. For consistency with the later simple evolution, the MWP radiative forcing from 0 to 1200 CE is chosen triangular-shaped with a maximum of 0.35 W m^{-2} at 600 CE (resulting in an SST amplitude comparable to Gebbie and Huybers (2019)). From 1200 CE the forcing is identical to the forcing in Fig. 1a.

Appendix B: Quantification of effects causing leads and lags at 3 km

500 ~~In this Appendix, we~~ [This Supplement is related to Sect. 3.4, which discusses the same effects only qualitatively. In this Section, we quantitatively](#) estimate the contribution of multiple effects on the deep ocean temperature at 3 kilometers. [Instead of a true decomposition, we present a rough estimate of each contribution.](#) This provides more insight in the origin of the leads and lags between TRA and FIX observed at 3 km in the different basins. The ~~end~~ results of these calculations are [summarized in Table ??, on which Table B3 of the main text is based. given in Table B3 and interpreted in Sect. B5.](#)

505 We are about to quantify the following effects:

1. changing SST
2. changing circulation:
 - 2a. water masses
 - 2b. water age

510 Throughout this Section, variables are only considered at the depth slice of 3.1 km, and within a certain basin, namely the Atlantic, Pacific or Southern Ocean (SO). Typically, variables are computed at steady state, $t_0 = 1200$ CE, or at a certain time step of interest, $t^* \in [1750, 2000]$ CE.

Temperature anomalies $T = T(t)$ at 3.1 km depth can be written in terms of water masses i :

$$T(t) = \sum_i T_i(t) \cdot f_i(t),$$

515 where $T_i(t)$ is the typical temperature of a certain water mass and $f_i(t)$ is this water mass' fraction between 0 and 1. The sum runs over all water masses $i \in [\text{NADW}, \text{NAIW}, \text{SAIW}, \text{SO}, \text{Arctic}, \text{NPIW}, \text{SPIW}, \text{Tropics}]$. This corresponds to our 8 dye tracers, which span the entire ocean surface (Fig. A1). Dropping the time dependence and writing $T_i(t)$ and $f_i(t)$ as a sum of their steady state at t_0 (subscript 0) and deviation (primed) yields

$$\begin{aligned}
 T &= \sum_i (T_{i,0} + T'_i) \cdot (f_{i,0} + f'_i) \\
 520 \quad &= \sum_i \underbrace{T_{i,0} \cdot f_{i,0}}_{\text{steady state}} + \underbrace{T'_i \cdot f_{i,0}}_{\text{1. changing SST}} + \underbrace{T_{i,0} \cdot f'_i}_{\text{2a. changing water masses}} + \underbrace{T'_i \cdot f'_i}_{\text{interaction}} \\
 &=: T_0 + \Delta T_{\text{SST}} + \Delta T_{\text{WM}} + \Delta T_{\text{int}}
 \end{aligned}$$

This decomposition is the main idea of this [Section Supplement](#). In the following, we reformulate the three rightmost terms one by one, making them more concrete such that we can compute them. The main outcomes are presented in the accompanying Tables; other used diagnosed values can readily be obtained from the available code (python notebook). [Results are summarized in Table B3 and their interpretation discussed in Sect. B5.](#)

525

B1 Effect 1: changing SST

First, we estimate the term corresponding to effect 1, changing SST, at a fixed time of interest t^* and depth 3.1 km by:

$$\Delta T_{\text{SST}}(t^*) \approx \sum_{i=1}^8 \overline{\Delta T}_i(t^*) \cdot f_i(t_0),$$

where f_i is the fraction of water mass i (between 0 and 1) taken as a basin average at the 3.1 km depth layer and computed at steady state t_0 . The average $\overline{\Delta T}_i(t^*)$ corresponds to the average surface temperature anomaly of dye tracer i averaged over the time interval $[t^* - a_{\text{max}}, t^* - a_{\text{min}}]$, where a_{min} and a_{max} are the minimum and maximum ideal age at 3.1 km depth occurring in the basin of interest. This is just one of the possible choices that can be made in order to estimate the history of surface temperatures $\overline{\Delta T}_i(t^*)$ that water mass i has seen at the times of subduction. This choice corresponds to picking a certain time interval in Fig. 1b before the time step of interest t^* , which should represent the times of subduction. Here we chose a non-weighted average over all possible times of subduction based on the ideal age tracer a . Note that this is an approximation, because the true age of, e.g., the NADW fraction of a certain water parcel is unknown. We only have the ideal age tracer at our disposal, which is the average over the entire probability density function of ages within a water parcel (grid cell) thus, e.g., also takes the age of the AABW fraction of this water parcel into account. A second assumption in our approach is taking the temperature of the surface where a water mass originates as the typical water mass temperature.

Writing out the averaging procedure,

$$\overline{\Delta T}_i(t^*) = \frac{1}{(t^* - a_{\text{min}}) - (t^* - a_{\text{max}})} \int_{t^* - a_{\text{max}}}^{t^* - a_{\text{min}}} \Delta T_i(t) dt$$

and combining this with the previous gives one final Equation for effect 1:

$$\Delta T_{\text{SST}}(t^*) \approx \frac{1}{a_{\text{max}}(t_0) - a_{\text{min}}(t_0)} \sum_{i=1}^8 f_i(t_0) \int_{t^* - a_{\text{max}}(t_0)}^{t^* - a_{\text{min}}(t_0)} \Delta T_i(t) dt \quad (\text{B1})$$

Here, we emphasized that a_{min} and a_{max} are diagnosed at time t_0 for effect 1. If either of the times at the integral boundaries occurs before the start of the simulation t_0 , then the values at t_0 are taken, which are representative since the ocean was in steady state before t_0 . The results of applying Eq. (B1) are shown in Table B1.

B2 Effect 2a: changing water masses

For effect 1, we multiplied the deviation in water mass temperature with the water mass fraction at steady state. For effect 2a, changing water masses, we now do the opposite: we take the product of the steady state water mass temperature with the deviation of the water mass fraction, again at a time of interest t^* and at depth 3.1 km. This gives us the change in temperature at 3.1 km due to water mass changes:

$$\Delta T_{\text{WM}}(t^*) \approx \sum_{i=1}^8 T_i(t_0) \cdot (f_i(t^*) - f_i(t_0)), \quad (\text{B2})$$

Table B1. Computing effect 1, changing SST. The six columns in the middle present a subset of the diagnosed values needed for the computation: as an example, only water masses NADW and SO and only $t^* = 2000$ are shown. The two rightmost columns show the result of effect 1 by using Eq. (B1), where all 8 water masses were taken into account.

Effect 1	$a_{\min}(t_0)^a$	$a_{\max}(t_0)^a$	$\overline{\Delta T_{\text{NADW}}(2000)}^b$	$\overline{\Delta T_{\text{SO}}(2000)}^b$	$f_{\text{NADW}}(t_0)$	$f_{\text{SO}}(t_0)$	$\Delta T_{\text{SST}}(1750)^b$	$\Delta T_{\text{SST}}(2000)^b$
Atlantic	13	746	-0.0242	-0.0419	0.580	0.307	-0.0485	-0.0333
Pacific	528	1397	0.00948	-0.00662	0.149	0.780	0.000108	-0.00462
SO	252	885	-0.0535	-0.0603	0.157	0.788	-0.00972	-0.0611

^a Ages a_{\min} and a_{\max} are in years.

^b Averaged temperatures $\overline{\Delta T_i}$ and results ΔT_{SST} are in $^{\circ}\text{C}$.

where $T_i(t_0)$ is the typical temperature of water mass i at steady state t_0 , based again on its surface temperature. Note that $T_i(t_0)$ relates to $\Delta T_i(t)$ in Eq. (B1) as $\Delta T_i(t) := T_i(t) - T_i(t_0)$. The results are shown in Table B2. The choice of basin does not influence T_i by definition, since the water mass temperature is diagnosed on its specific surface (Fig. A1).

Table B2. Computing effect 2a, changing water masses. The six columns in the middle present a subset of the diagnosed values needed for the computation: as an example, only water masses NADW and SO are shown. In addition, $f_i(t_0)$ from Table B1 are used. The two rightmost columns show the result of effect 2a by using Eq. (B2), where all 8 water masses were taken into account.

Effect 2a	$T_{\text{NADW}}(t_0)^a$	$T_{\text{SO}}(t_0)^a$	$f_{\text{NADW}}(1750)$	$f_{\text{SO}}(1750)$	$f_{\text{NADW}}(2000)$	$f_{\text{SO}}(2000)$	$\Delta T_{\text{WM}}(1750)^a$	$\Delta T_{\text{WM}}(2000)^a$
Atlantic	5.486	2.732	0.584	0.301	0.568	0.319	0.0352	-0.0203
Pacific	5.486	2.732	0.148	0.783	0.148	0.783	-0.0113	-0.0134
SO	5.486	2.732	0.154	0.793	0.159	0.786	-0.0290	0.0222

^aTemperatures are in $^{\circ}\text{C}$.

B3 Effect 2b: changing water age

Changing ocean circulation consists of the combined effect of a) changing water masses (diagnosed by dye tracers) and b) changing water age (diagnosed by the ideal age tracer). If we adapt the simplified view of two deep water formation end members or pumps, located in the North Atlantic and in the Southern Ocean, then this distinction corresponds to a) changing the ocean volume filled by each pump (one of the pumps fills more of the ocean volume and the other less) and b) both pumps

increase (decrease) equally in strength such that they turn over faster (slower) within their own overturning cell, which causes a younger (older) water age. It is in principle possible that one of these effects occurs independently without the other, but in reality they typically occur simultaneously and are hard to separate; when an overturning cell increases or decreases in strength, it usually also becomes deeper or shallower. We try this separation nevertheless and estimate the effect of changing water age, representing absolute overturning rate.

Changing water age alters effect 1, changing SST. Since the ages a_{\min} and a_{\max} shift towards younger (older) values under stronger (weaker) absolute overturning, the average $\overline{\Delta T}(t_0)$ in Eq. (B1) must now be evaluated at t^* instead of t_0 . This gives the effect of water age

$$\Delta T_{\text{WA}}(t^*) \approx \left(\frac{1}{a_{\max}(t^*) - a_{\min}(t^*)} \sum_{i=1}^8 f_i(t_0) \int_{t^* - a_{\max}(t^*)}^{t^* - a_{\min}(t^*)} \Delta T_i(t) dt \right) - \Delta T_{\text{SST}}(t^*), \quad (\text{B3})$$

where we subtracted effect 1 in order to find only the adjustment due to effect 2b. Since the resulting contribution of water age changes $\Delta T_{\text{WA}}(t^*)$ is relatively small, the diagnosed values of $a_{\min}(t^*)$, $a_{\max}(t^*)$ and $\overline{\Delta T}_i(t^*)$ needed for the calculation are not shown here. The result $\Delta T_{\text{WA}}(t^*)$ is displayed directly in summary Table [B3](#) in cK.

B4 Interaction

The interaction is small, but computed for completeness by combining the deviations of T_i and f_i and summing again over all water masses i :

$$\Delta T_{\text{int}}(t^*) \approx \sum_{i=1}^8 \overline{\Delta T}_i(t^*) \cdot (f_i(t^*) - f_i(t_0)) \quad (\text{B4})$$

All quantities required for this were already diagnosed and (partly) shown in Table B1 and Table B2. The result of Eq. (B4) is directly shown below in the respective column in Table [B3](#).

B5 **Summarizing the Final results and interpretation**

We summarize the above and compare the contribution of each effect in Table [B3](#). ~~Table B3 of the main text follows from Table [B3](#), by converting Celsius to centi-Kelvin, by rounding to 2 significant figures with a maximum of 3 decimals and by adding percentages. [This Table summarizes how much each of the effects, which are discussed qualitatively in Sect. 3.4, quantitatively impacts total deep ocean temperature anomalies, although uncertainties are large \(indicated by the Residual column; discussion of uncertainty in Sect. B6\).](#)~~

Firstly, the effect of SST history (effect 1) at a fixed 3.1 km depth contributes a cooling in 1750 CE in the deep Atlantic and SO, but no SST-caused cooling reaches the deep Pacific yet. In 2000 CE, the cooling contribution reached the deep Pacific and is still present at this depth in the other basins.

Secondly, Table B3 confirms the expectation in Sect. 3.4, based on NADW and SO dye tracers, that in 1750 effect 2a (shifting water masses) leads to a warming in the Atlantic and a cooling in the Pacific at 3.1 km. Note that now all 8 water masses are

590 taken into account such that a second-order effect is present: relatively more deep water formation water masses (NADW and AABW) relative to other water masses under the LIA forcing, which leads to an additional cooling. In the year 2000, we see a cooling in the Atlantic and Pacific at this depth, again confirming the expectations from dye tracers in Sect. 3.4, whereas the SO warms. Water mass anomalies in 2000 south of 35°S (Fig. 8 and 9) show that the SO warming is caused by more NADW-sourced water and less local SO water.

595 For effect 2b, many values in Table B3 have different signs than expected from the analysis of small ideal age anomalies in Sect. 3.4. We conclude that the values indicated as $< 2\%$ are indeed not significantly different from zero. Thus, effect 2b has a very small impact at 3.1 km, except in the case of the Atlantic in 2000, where we also observed the largest change in ideal age.

Finally, we compare the relative contributions of effects 1, 2a and 2b. The change in absolute overturning rate, which is
600 estimated via water age, has practically no influence in all cases except the Atlantic in 2000 CE, where the largest overturning anomalies take place. In all other cases, deep ocean temperature anomalies are determined by the interplay of SST and water mass changes. In the Atlantic, SST and water mass changes contribute roughly equally in 1750 but with opposite signs. Therefore, the shifted water masses cause a delay in the arrival of LIA cooling at depth until 1750. In 2000, both water masses and water ages now strongly enhance the amplitude of the cooling, which arrives relatively late. As such, the arrival of the
605 industrial warming is delayed as well. These mechanisms explain the two-century lag observed in the Atlantic and nicely correspond to Fig. 4d, where we see the amplitude of TRA dampened until 1750 but enhanced until 2000 (and further in time). In the Pacific and SO, the contribution of water mass changes generally dominates over SST (except for the SO in 2000). These water mass changes contribute with the same sign as the forcing such that they fasten and enhance the arrival of anomalies at depth. This explains the leads observed in the Pacific and SO and the larger amplitudes in TRA.

610 **B6 Uncertainty**

Finally, we make a few closing remarks about uncertainty.

We note that the estimate of effect 1 (changing SST) has a large uncertainty, which explains a substantial amount in the residual column. This is due to the usage of the ideal age tracer as estimate for the age of a specific water mass, as mentioned above. For example: a water parcel with 75 % NADW with age 200 years and 25 % AABW with age 600 years gives an ideal
615 age of 300 years. In this example, effect 1 is estimated with an NADW age of 300 years and an AABW age of 300 years. This uncertainty of effect 1 can be quantified, because we can also compute effect 1 directly from the output of OcFIX, which gives the ‘perfect’ SST contribution, i.e., exactly as simulated in the Bern3D model. For completion, we list the values of the perfect SST contribution here, in the same order as the rows in Table ~~??~~B3: -0.00452, -0.0125, -0.0507, -0.0680, -0.017 and -0.0265 °C. Using these perfect values for the SST contribution would result in better residual values: -0.0100, -0.0136,
620 0.0040, 0.0018, -0.0163 and 0.0115 °C. We did not use these values for consistency reasons, as they do not correspond to the estimates for effect 2b, which is based on effect 1. We conclude that in most cases one third to two thirds of the residual is explained by the uncertainty in effect 1.

Effect 2a (changing water masses) is thought to be well-known, since it does not use the ideal age tracer to estimate water mass age. The uncertainty in effect 1 propagates in effect 2b (changing water ages), since it is based on effect 1. As an uncertainty estimate for effect 2b, we take the percentage uncertainty in the SST contribution quantified above and take the same percentage as uncertainty for effect 2b. This gives an uncertainty of roughly 200 % to 300 % for most basins and most time steps. Note that this uncertainty is not symmetric, since the SST estimate is generally too small thus we also expect effect 2b to be too small rather than too large (in absolute values). Scaling the percentage contribution of effect 2b (Table B3) by a factor of 2 or 3 typically changes values of 2 % to maximally 6 % hence still very small. We conclude that the uncertainty in effect 2b is large, but this does not change our main message of effect 2b being small in all cases, except perhaps in the Atlantic in 2000 CE.

Table B3. Summary of quantification of how different effects act on the deep ocean temperature at 3.1 km, per basin and at times of interest 1750 CE and 2000 CE. All values are temperature anomalies w.r.t. 1200 CE in centi-Kelvin (cK). Percentages are added in parentheses, where the residual is excluded, i.e., 100 % corresponds to the sum of effects 1, 2a, 2b and their interaction. For the percentage, the absolute value of each contribution is taken.

Multiple effects @3.1 km on:		1. Changing SST ^a 1. History of SST	2. Changing circulation ^b 2a. Water masses ^c	2b. Water age ^d	Interaction ^e	Residual ^f
Atlantic:	1750	<u>-0.0485</u> -4.9 (57%)	<u>0.0352</u> -3.5 (41%)	<u>-0.00168</u> -17 (2%)	<u>-0.00004</u> -0.004 (0%)	<u>0.00178</u> -0.18
	2000	<u>-0.0333</u> -3.3 (32%)	<u>-0.0203</u> -2.0 (19%)	<u>-0.0498</u> -5.0 (48%)	<u>-0.00025</u> -0.25 (0%)	<u>-0.03687</u> -3.7
Pacific:	1750	<u>0.000108</u> -0.011 (1%)	<u>-0.0113</u> -1.1 (97%)	<u>0.000233</u> -0.023 (2%)	<u>-0.00001</u> -0.001 (0%)	<u>-0.01462</u> -1.5
	2000	<u>-0.00462</u> -46 (26%)	<u>-0.0134</u> -1.3 (72%)	<u>-0.000375</u> -0.38 (2%)	<u>-0.00002</u> -0.002 (0%)	<u>-0.02152</u> -2.2
Southern Ocean:	1750	<u>-0.00972</u> -97 (25%)	<u>-0.0290</u> -2.9 (74%)	<u>-0.000587</u> -0.59 (1%)	<u>-0.00006</u> -0.006 (0%)	<u>-0.02541</u> -2.5
	2000	<u>-0.0611</u> -6.1 (73%)	<u>0.0222</u> -2.2 (26%)	<u>0.0000831</u> -0.008 (0%)	<u>-0.00006</u> -0.006 (0%)	<u>0.04606</u> -4.6

^aResults are taken over from Table B1 and converted to cK.

^bChanging circulation consists of the – not necessarily independent – subeffects 2a and 2b.

^cResults are taken over from Table B2 and converted to cK.

^dThe water-age contribution follows from Eq. (B3).

^eThe interaction is the cross term of deviations between effect 1 and 2a and follows from Eq. (B4).

^fThe residual equals the total minus effects 1, 2a, 2b and the interaction. It represents unaccounted effects and uncertainties in the calculations.

^gThe total of all effects is given by the model output $\Delta T := T(t^*) - T(t_0)$ of OcTRA, which is averaged at 3.1 km within the basin of interest.

Author contributions. J.S. carried out the numerical simulations, implementation and analysis. T.F.S. conceived the original idea and supervised the project. J.S. lead the writing of the manuscript. Both authors contributed to the interpretation of the results.

Competing interests. The authors declare that they have no conflict of interest.

635 *Acknowledgements.* This work is supported by the Swiss National Science Foundation by grant SNF 200020_172745. We [thank Woon Mi Kim and Angelique Hameau for providing sea surface salinity output of CESM1.0.1 during the past millennium. We](#) gratefully acknowledge Thomas L. Frölicher for helpful comments on an earlier version of the manuscript ~~—~~[and two anonymous reviewers for their constructive feedback, which improved the paper. We thank G. Gebbie for providing the data for Fig. 11c and details on their analysis.](#)

References

- 640 Abraham, J. P., Baringer, M., Bindoff, N. L., Boyer, T., Cheng, L. J., Church, J. A., Conroy, J. L., Domingues, C. M., Fasullo, J. T., Gilson, J., Goni, G., Good, S. A., Gorman, J. M., Gouretski, V., Ishii, M., Johnson, G. C., Kizu, S., Lyman, J. M., Macdonald, A. M., Minkowycz, W. J., Moffitt, S. E., Palmer, M. D., Piola, A. R., Reseghetti, F., Schuckmann, K., Trenberth, K. E., Velicogna, I., and Willis, J. K.: A review of global ocean temperature observations: Implications for ocean heat content estimates and climate change, *Reviews of Geophysics*, 51, 450–483, <https://doi.org/10.1002/rog.20022>, 2013.
- 645 Banks, H. T. and Gregory, J. M.: Mechanisms of ocean heat uptake in a coupled climate model and the implications for tracer based predictions of ocean heat uptake, *Geophysical Research Letters*, 33, <https://doi.org/10.1029/2005GL025352>, 2006.
- Brönnimann, S., Franke, J., Nussbaumer, S., Zumbühl, H., Steiner, D., Trachsel, M., Hegerl, G., Schurer, A., Worni, M., Malik, A., Flückiger, J., and Raible, C.: Last phase of the Little Ice Age forced by volcanic eruptions, *Nature Geoscience*, 12, <https://doi.org/10.1038/s41561-019-0402-y>, 2019.
- 650 Collins, M., Sutherland, M., Bouwer, L., Cheong, S.-M., Frölicher, T., Jacot Des Combes, H., Koll Roxy, M., Losada, I., McInnes, K., Ratter, B., Rivera-Arriaga, E., Susanto, R. D., Swingedouw, D., and Tibig, L.: Extremes, Abrupt Changes and Managing Risk, in: IPCC Special Report on the Ocean and Cryosphere in a Changing Climate, edited by Pörtner, H.-O., Roberts, D. C., Masson-Delmotte, V., Zhai, P., Tignor, M., Poloczanska, E., Mintenbeck, K., Alegría, A., Nicolai, M., Okem, A., Petzold, J., Rama, B., and Weyer, N., In press, <https://www.ipcc.ch/srocc/chapter/chapter-6/>, 2019.
- 655 Edwards, N. R., Willmott, A. J., and Killworth, P. D.: On the Role of Topography and Wind Stress on the Stability of the Thermohaline Circulation, *Journal of Physical Oceanography*, 28, 756–778, [https://doi.org/10.1175/1520-0485\(1998\)028<0756:OTROTA>2.0.CO;2](https://doi.org/10.1175/1520-0485(1998)028<0756:OTROTA>2.0.CO;2), 1998.
- Emile-Geay, J., McKay, N., Kaufman, D., Von Gunten, L., Wang, J., Anchukaitis, K., Abram, N., Addison, J., Curran, M., Evans, M., Henley, B., Hao, Z., Martrat, B., McGregor, H., Neukom, R., Pederson, G., Stenni, B., Thirumalai, K., Werner, J., and Zinke, J.: A global multiproxy database for temperature reconstructions of the Common Era, *Scientific Data*, 4, 170 088, <https://doi.org/10.1038/sdata.2017.88>, 2017.
- 660 England, M. H.: The Age of Water and Ventilation Timescales in a Global Ocean Model, *Journal of Physical Oceanography*, 25, 2756–2777, [https://doi.org/10.1175/1520-0485\(1995\)025<2756:TAOWAV>2.0.CO;2](https://doi.org/10.1175/1520-0485(1995)025<2756:TAOWAV>2.0.CO;2), 1995.
- Garuba, O. A. and Klinger, B. A.: Ocean Heat Uptake and Interbasin Transport of the Passive and Redistributive Components of Surface Heating, *Journal of Climate*, 29, 7507–7527, <https://doi.org/10.1175/JCLI-D-16-0138.1>, 2016.
- 665 Gebbie, G. and Huybers, P.: The Mean Age of Ocean Waters Inferred from Radiocarbon Observations: Sensitivity to Surface Sources and Accounting for Mixing Histories, *Journal of Physical Oceanography*, 42, 291–305, <https://doi.org/10.1175/JPO-D-11-043.1>, 2012.
- Gebbie, G. and Huybers, P.: The Little Ice Age and 20th-century deep Pacific cooling, *Science*, 363, 70–74, <https://doi.org/10.1126/science.aar8413>, 2019.
- Hall, T. and Haine, T.: On Ocean Transport Diagnostics: The Idealized Age Tracer and the Age Spectrum, *Journal of Physical Oceanography*, 32, 1987–1991, [https://doi.org/10.1175/1520-0485\(2002\)032<1987:OOTDTI>2.0.CO;2](https://doi.org/10.1175/1520-0485(2002)032<1987:OOTDTI>2.0.CO;2), 2002.
- 670 Levin, L. A., Bett, B. J., Gates, A. R., Heimbach, P., Howe, B. M., Janssen, F., McCurdy, A., Ruhl, H. A., Snelgrove, P., Stocks, K. I., Bailey, D., Baumann-Pickering, S., Beaverson, C., Benfield, M. C., Booth, D. J., Carreiro-Silva, M., Colaço, A., Eblé, M. C., Fowler, A. M., Gjerde, K. M., Jones, D. O. B., Katsumata, K., Kelley, D., Le Bris, N., Leonardi, A. P., Lejzerowicz, F., Macreadie, P. I., McLean, D., Meitz, F., Morato, T., Netburn, A., Pawlowski, J., Smith, C. R., Sun, S., Uchida, H., Vardaro, M. F., Venkatesan, R., and Weller, R. A.: Global Observing Needs in the Deep Ocean, *Frontiers in Marine Science*, 6, 241, <https://doi.org/10.3389/fmars.2019.00241>, 2019.

- Mann, M., Bradley, R., and Hughes, M.: Global-Scale Temperature Patterns and Climate Forcing Over the Past Six Centuries, *Nature*, 392, 779–787, <https://doi.org/10.1038/33859>, 1998.
- Mann, M. E., Zhang, Z., Rutherford, S., Bradley, R. S., Hughes, M. K., Shindell, D., Ammann, C., Faluvegi, G., and Ni, F.: Global Signatures and Dynamical Origins of the Little Ice Age and Medieval Climate Anomaly, *Science*, 326, 1256–1260, <https://doi.org/10.1126/science.1177303>, 2009.
- 680 Marshall, J., Scott, J., Armour, K., Campin, J.-M., Kelley, M., and Romanou, A.: The ocean’s role in the transient response of climate to abrupt greenhouse gas forcing, *Climate Dynamics*, 44, <https://doi.org/10.1007/s00382-014-2308-0>, 2015.
- Masson-Delmotte, V., Schulz, M., Abe-Ouchi, A., Beer, J., Ganopolski, A., González Rouco, J. F., Jansen, E., Lambeck, K., Luterbacher, J., Naish, T., Osborn, T., Otto-Bliesner, B., Quinn, T., Ramesh, R., Rojas, M., Shao, X., and Timmermann, A.: Chapter 5: Information from Paleoclimate Archives, in: *Climate Change 2013: The Physical Science Basis*, edited by Stocker, T. F., Qin, D., Plattner, G.-K., Tignor, M., Allen, S. K., Boschung, J., Nauels, A., Xia, Y., Bex, V., and Midgley, P. M., Contribution of Working Group I to the Fifth Assessment Report of the Intergovernmental Panel on Climate Change, p. 383–464, Cambridge University Press, https://archive.ipcc.ch/pdf/assessment-report/ar5/wg1/WG1AR5_Chapter05_FINAL.pdf, 2013.
- 685 McGregor, H. V., Evans, M. N., Goosse, H., Leduc, G., Martrat, B., Addison, J. A., Mortyn, P. G., Oppo, D. W., Seidenkrantz, M.-S., Sicre, M.-A., Phipps, S. J., Selvaraj, K., Thirumalai, K., Filipsson, H. L., and Ersek, V.: Robust global ocean cooling trend for the pre-industrial Common Era, *Nature Geoscience*, 8, 671, <https://doi.org/https://doi.org/10.1038/ngeo2510> 10.1038/ngeo2510, 2015.
- Moffa-Sánchez, P., Moreno-Chamarro, E., Reynolds, D. J., Ortega, P., Cunningham, L., Swingedouw, D., Amrhein, D. E., Halfar, J., Jonkers, L., Jungclaus, J. H., Perner, K., Wanamaker, A., and Yeager, S.: Variability in the Northern North Atlantic and Arctic Oceans Across the Last Two Millennia: A Review, *Paleoceanography and Paleoclimatology*, 34, 1399–1436, <https://doi.org/10.1029/2018PA003508>, 2019.
- 695 Müller, S. A., Joos, F., Edwards, N. R., and Stocker, T. F.: Water Mass Distribution and Ventilation Time Scales in a Cost-Efficient, Three-Dimensional Ocean Model, *Journal of Climate*, 19, 5479–5499, <https://doi.org/10.1175/JCLI3911.1>, 2006.
- Neukom, R., Steiger, N., Gómez-Navarro, J. J., Wang, J., and Werner, J. P.: No evidence for globally coherent warm and cold periods over the preindustrial Common Era, *Nature*, 571, 550–554, <https://doi.org/10.1038/s41586-019-1401-2>, 2019.
- PAGES 2k Consortium: Continental-scale temperature variability during the past two millennia, *Nature Geoscience*, 6, 339–346, <https://doi.org/10.1038/ngeo1834>, 2013.
- 700 Rayner, N. A., Parker, D. E., Horton, E. B., Folland, C. K., Alexander, L. V., Rowell, D. P., Kent, E. C., and Kaplan, A.: Global analyses of sea surface temperature, sea ice, and night marine air temperature since the late nineteenth century, *Journal of Geophysical Research: Atmospheres*, 108, <https://doi.org/10.1029/2002JD002670>, 2003.
- Ritz, S. P., Stocker, T. F., and Joos, F.: A Coupled Dynamical Ocean-Energy Balance Atmosphere Model for Paleoclimate Studies, *Journal of Climate*, 24, 349–375, <https://doi.org/10.1175/2010JCLI3351.1>, 2011.
- 705 Roth, R., Ritz, S. P., and Joos, F.: Burial-nutrient feedbacks amplify the sensitivity of atmospheric carbon dioxide to changes in organic matter remineralisation, *Earth System Dynamics*, 5, 321–343, <https://doi.org/10.5194/esd-5-321-2014>, 2014.
- Scheen, J.: Effect of changing ocean circulation on deep ocean temperature in the last millennium: code, <https://doi.org/10.5281/zenodo.4022947>, 2020.
- 710 Scheen, J., Gebbie, G., and Stocker, T. F.: Effect of changing ocean circulation on deep ocean temperature in the last millennium: simulation output data, <https://doi.org/10.5281/zenodo.4022927>, 2020.
- Steiger, N., Smerdon, J., Cook, E., and Cook, B.: A reconstruction of global hydroclimate and dynamical variables over the Common Era, *Scientific Data*, 5, 180086, <https://doi.org/10.1038/sdata.2018.86>, 2018.

- Winton, M., Griffies, S. M., Samuels, B. L., Sarmiento, J. L., and Frölicher, T. L.: Connecting Changing Ocean Circulation with Changing
715 Climate, *Journal of Climate*, 26, 2268–2278, <https://doi.org/10.1175/JCLI-D-12-00296.1>, 2013.
- Xie, P. and Vallis, G.: The passive and active nature of ocean heat uptake in idealized climate change experiments, *Climate Dynamics*, 38,
667–684, <https://doi.org/10.1007/s00382-011-1063-8>, 2011.